

## Integrating continuous atmospheric boundary layer and tower-based flux measurements to advance understanding of land-atmosphere interactions



Manuel Helbig<sup>a,\*</sup>, Tobias Gerken<sup>b</sup>, Eric R. Beamesderfer<sup>c,aa</sup>, Dennis D. Baldocchi<sup>d</sup>, Tirtha Banerjee<sup>e</sup>, Sébastien C. Biraud<sup>f</sup>, William O.J. Brown<sup>g</sup>, Nathaniel A. Brunsell<sup>h</sup>, Elizabeth A Burakowski<sup>i</sup>, Sean P. Burns<sup>g,j</sup>, Brian J. Butterworth<sup>k</sup>, W. Stephen Chan<sup>f</sup>, Kenneth J. Davis<sup>l,m</sup>, Ankur R. Desai<sup>k</sup>, Jose D. Fuentes<sup>l</sup>, David Y. Hollinger<sup>n</sup>, Natascha Kljun<sup>o</sup>, Matthias Mauder<sup>p</sup>, Kimberly A. Novick<sup>q</sup>, John M. Perkins<sup>r</sup>, David A. Rahn<sup>h</sup>, Camilo Rey-Sánchez<sup>d</sup>, Joseph A. Santanello<sup>s</sup>, Russell L. Scott<sup>t</sup>, Bijan Seyednasrollah<sup>c</sup>, Paul C. Stoy<sup>u</sup>, Ryan C. Sullivan<sup>v</sup>, Jordi Vilà-Guerau de Arellano<sup>w</sup>, Sonia Wharton<sup>x</sup>, Chuixiang Yi<sup>y,z</sup>, Andrew D. Richardson<sup>c,aa</sup>

<sup>a</sup> Department of Physics and Atmospheric Science, Dalhousie University, Halifax, NS, Canada

<sup>b</sup> School of Integrated Sciences, James Madison University, Harrisonburg, VA, USA

<sup>c</sup> School of Informatics, Computing and Cyber Systems, Northern Arizona University, Flagstaff, AZ, USA

<sup>d</sup> Department of Environmental Science, Policy, and Management, University of California-Berkeley, Berkeley, CA, USA

<sup>e</sup> Department of Civil and Environmental Engineering, University of California-Irvine, Irvine, CA, USA

<sup>f</sup> Earth and Environmental Sciences Area, Lawrence Berkeley National Laboratory, Berkeley, CA, USA

<sup>g</sup> National Center for Atmospheric Research, Boulder, CO, USA

<sup>h</sup> Department of Geography and Atmospheric Science, University of Kansas, Lawrence, KS, USA

<sup>i</sup> Institute for the Study of Earth, Oceans, and Space, University of New Hampshire, Durham, NH, USA

<sup>j</sup> Department of Geography, University of Colorado, Boulder, CO, USA

<sup>k</sup> Department of Atmospheric and Oceanic Sciences, University of Wisconsin-Madison, Madison, WI, USA

<sup>l</sup> Department of Meteorology and Atmospheric Science, The Pennsylvania State University, University Park, PA, USA

<sup>m</sup> Earth and Environmental Systems Institute, The Pennsylvania State University, University Park, PA, USA

<sup>n</sup> USDA Forest Service, Northern Research Station, Durham, NC, USA

<sup>o</sup> Centre for Environmental and Climate Science, Lund University, Sweden

<sup>p</sup> Institute of Meteorology and Climate Research - Atmospheric Environmental Research (IMK-IFU), Karlsruhe Institute of Technology, Garmisch-Partenkirchen, Germany

<sup>q</sup> O'Neill School of Public and Environmental Affairs, Indiana University - Bloomington, Bloomington, IN, USA

<sup>r</sup> Department of Hydrology and Atmosphere Sciences, University of Arizona, Tucson, AZ, USA

<sup>s</sup> Hydrological Sciences Laboratory, NASA-GSFC, Greenbelt, MD, USA

<sup>t</sup> Southwest Watershed Research Center, USDA-Agricultural Research Service, Tucson, AZ, USA

<sup>u</sup> Department of Biological Systems Engineering, University of Wisconsin-Madison, Madison, WI, USA

<sup>v</sup> Environmental Science Division, Argonne National Laboratory, Lemont, IL, USA

<sup>w</sup> Meteorology and Air Quality Section, Wageningen University, Wageningen, The Netherlands

<sup>x</sup> Atmospheric, Earth and Energy Division, Lawrence Livermore National Laboratory, Livermore, CA, USA

<sup>y</sup> School of Earth and Environmental Sciences, Queens College, City University of New York, New York, NY, USA

<sup>z</sup> Earth and Environmental Sciences Department, Graduate Center, City University of New York, New York, NY 10016, USA

<sup>aa</sup> Center for Ecosystem Science and Society, Northern Arizona University, Flagstaff, AZ, USA

### ARTICLE INFO

### ABSTRACT

#### Keywords:

Eddy covariance

Boundary layer

Land-atmosphere

Remote sensing

Atmospheric inversion

The atmospheric boundary layer mediates the exchange of energy, matter, and momentum between the land surface and the free troposphere, integrating a range of physical, chemical, and biological processes and is defined as the lowest layer of the atmosphere (ranging from a few meters to 3 km). In this review, we investigate how continuous, automated observations of the atmospheric boundary layer can enhance the scientific value of co-located eddy covariance measurements of land-atmosphere fluxes of carbon, water, and energy, as are being made at FLUXNET sites worldwide. We highlight four key opportunities to integrate tower-based flux

\* Corresponding author.

E-mail address: [manuel.helbig@dal.ca](mailto:manuel.helbig@dal.ca) (M. Helbig).

measurements with continuous, long-term atmospheric boundary layer measurements: (1) to interpret surface flux and atmospheric boundary layer exchange dynamics and feedbacks at flux tower sites, (2) to support flux footprint modelling, the interpretation of surface fluxes in heterogeneous and mountainous terrain, and quality control of eddy covariance flux measurements, (3) to support regional-scale modeling and upscaling of surface fluxes to continental scales, and (4) to quantify land-atmosphere coupling and validate its representation in Earth system models. Adding a suite of atmospheric boundary layer measurements to eddy covariance flux tower sites, and supporting the sharing of these data to tower networks, would allow the Earth science community to address new emerging research questions, better interpret ongoing flux tower measurements, and would present novel opportunities for collaborations between FLUXNET scientists and atmospheric and remote sensing scientists.

## 1. Introduction

The land-atmosphere exchange of energy, matter, and momentum has been measured using the eddy covariance technique since the late 1960's (e.g., Hicks and Martin, 1972; Kaimal and Wyngaard, 1990, McKay and Thurtell, 1978; Leuning et al., 1982; Desjardins et al., 1984; Baldocchi et al., 1988). Since then, the number of eddy covariance flux tower sites has increased substantially, thus improving the spatial and temporal coverage of land-atmosphere exchange observations across the globe (e.g., Chu et al., 2017; Novick et al., 2018; Keenan et al., 2019). As of 2019, eddy covariance-based flux measurements have been conducted at more than 2000 sites located on all continents (Burba, 2019). An international network of flux tower sites called FLUXNET has emerged over the past few decades resulting in multi-site and multi-year datasets (Baldocchi, 2020; Pastorello et al., 2020). Many of the sites in FLUXNET are now providing open access data to users worldwide. FLUXNET efforts have focused on measuring biospheric fluxes of carbon dioxide ( $\text{CO}_2$ ), water vapor, latent and sensible heat, while more recent efforts aim to produce similar datasets for methane fluxes (Knox et al., 2019). The wealth of eddy covariance-based flux observations has advanced our understanding of land-atmosphere interactions (e.g., role of diffuse radiation on ecosystem carbon uptake (Niyogi et al., 2004; Knoll and Baldocchi, 2008), effect of increasing atmospheric  $\text{CO}_2$  concentrations on water-use efficiency (Keenan et al., 2013), thermal optimality of net ecosystem carbon exchange (Niu et al., 2012), and the effect of increasing vapor pressure deficit on carbon and water fluxes (Novick et al., 2016). FLUXNET data have also proven invaluable for benchmarking and testing ecosystem models (e.g., Bonan et al., 2011; Collier et al., 2018), and validating remotely sensed information about land surface function (e.g., Zhao et al., 2005; Heinsch et al., 2006; Schimel et al., 2015). However, most studies using eddy covariance-based flux observations have focused on ecosystem responses to atmospheric (e.g., air temperature and humidity,  $\text{CO}_2$  concentrations), environmental (e.g., soil moisture), ecological (e.g., wildfire and insect disturbances), or anthropogenic drivers (e.g., anthropogenic disturbances, land management), while fewer studies have addressed complex interactions between land and atmospheric processes (e.g., Juang et al., 2007a; Lee et al., 2011; Baldocchi and Ma, 2013; Sanchez-Mejia and Papuga, 2014; Burns et al., 2015; Rigden and Li, 2017; Brugger et al., 2018; Gerken et al., 2019; Lansu et al., 2020; Helbig et al., 2020a).

The interactions between the land surface and atmosphere are mostly confined to the atmospheric boundary layer (ABL, e.g., Yi et al., 2004), commonly defined as the lowest layer of the atmosphere (depth varies from a few meters to 1-3 km), which is directly influenced by land surface processes. The ABL links properties of soils, vegetation, and urban landscapes to the free troposphere and is of critical importance for weather, climate, and pollutant dispersion and chemistry. For example, land-atmosphere feedback mechanisms (e.g., Raupach, 1998) exert important controls on global carbon storage dynamics (e.g., Green et al., 2019; Humphrey et al., 2021), soil moisture availability (e.g., Shi et al., 2013; Vogel et al., 2017), water balance (e.g., McNaughton and Spriggs, 1986; Salvucci and Gentile, 2013), surface energy balance (e.g., Lansu et al., 2020), cloud formation and patterns (e.g., Siqueira et al., 2009;

Vilà-Guerau de Arellano et al., 2012), atmospheric chemistry and air pollution (e.g., Janssen et al., 2013), and future climate change trajectories (e.g., Davy and Esau, 2016). Additionally, the state of the lower atmosphere contains information that can constrain observations of land surface processes and states (e.g., plant photosynthesis and respiration (Denning et al., 1999; Lauvau et al., 2012), soil water availability (Salvucci and Gentile, 2013). However, continuous ABL observations with sufficient vertical resolution are currently not available globally from spaceborne remote sensing and are rarely collected across the FLUXNET network even though the advantages of having co-located surface flux, radiation, humidity, and other ABL measurements are numerous.

In this review paper, we explore how extending co-located ABL observations (e.g., from radiosondes, ceilometers, and lidar or radar profilers) across the FLUXNET network could improve our mechanistic understanding of land-atmosphere interactions and feedbacks. First, we discuss typical diurnal ABL dynamics, then we give a brief overview of available ABL observation systems and of current ABL observation efforts at flux towers. We conclude with a discussion of new research opportunities that could emerge from an expansion of ABL observations across the FLUXNET network.

## 2. Background

### 2.1. Typical diurnal atmospheric boundary layer evolution

During daytime, the ABL is frequently well-mixed (above the roughness sublayer and the surface layer) and bounded by the land surface at its lower boundary and by a capping thermal inversion at its upper boundary (e.g., Wouters et al., 2019; Table 1). The capping inversion can be detected as the maximum positive vertical gradient of potential temperature and minimum negative gradient of specific humidity, separating the ABL from the free troposphere (Fig. 1 and 2). The lowest layer of the ABL is the roughness sublayer (Fig. 3), which has traditionally been defined as the layer immediately above the surface wherein surface roughness elements (i.e., trees, buildings) induce horizontal variability of time-averaged flow (Mahrt, 2000). Above an extended homogeneous surface, the top of the roughness sublayer can be thought of as the (local) 'blending height' and indicates the height above which the influence of surface roughness elements and surface heterogeneity decrease. The depth of the roughness sublayer depends on surface properties, including roughness length, roughness element spacing, height, and area shape of roughness elements, but is typically 2-5 times the height of the roughness elements (Raupach et al., 1991; Fig. 3). The roughness sublayer is overlain by the surface layer, which usually extends to about 10% of the ABL height. In the surface layer, wind and temperature profiles are often well-described as logarithmic functions of height (i.e., Monin-Obukhov Similarity Theory functions, Monin and Obukhov, 1954) and turbulent fluxes are nearly constant with height (also called the constant flux layer). In contrast, vertical profiles of wind and temperature in the roughness sublayer usually deviate from profiles predicted by Monin-Obukhov Theory (Fig. 3) since turbulence characteristics depend on the influence of individual roughness elements (Raupach and Thom, 1981). Over heterogeneous surfaces, the regional

**Table 1**

List of definitions.

Term	Definition
<i>Adiabatic process</i>	No external heat is transferred to an air parcel (e.g., adiabatic cooling of a rising air parcel due to decreasing pressure).
<i>Atmospheric boundary layer [ABL] (or planetary boundary layer)</i>	Lower layer of the troposphere, which is directly influenced by the planetary surface. Roughly a few meters to 1–3 km.
<i>Atmospheric boundary layer height (or mixing height) [ABLH]</i>	Thickness of the atmospheric boundary layer often characterized by a temperature inversion at the top of the ABL. During daytime, the ABLH typically responds to surface forcing within a time scale of an hour to a few hours. In some cases, ABL growth may be capped by atmospheric subsidence. Mixing height refers to the height up to which heat, matter, and momentum originating from the land surface are well mixed (above the roughness sublayer and the surface layer) through turbulent vertical mixing.
<i>Capping inversion</i>	Elevated inversion layer (i.e., reversal of temperature gradient) at the top of the ABL separating ABL from free troposphere
<i>Convective boundary layer (or daytime boundary layer, mixed layer) [CBL]</i>	Type of ABL that is characterized by vigorous turbulence and mixing due to heating at the bottom of the ABL and entrainment at the top of the ABL during the day.
<i>Entrainment</i>	Process by which the turbulent mixed layer incorporates less turbulent air from the free troposphere leading to deepening of the mixed layer. Entrainment zone shear enhances entrainment and can contribute to rapid ABL growth. Typically, entrainment is associated with warming and drying of the ABL.
<i>Free troposphere</i>	Atmospheric layer above the ABL where the influence of the planetary surface (surface friction/drag) is minimal. Air in the free troposphere is warmer (for potential air temperature) and drier than in the ABL.
<i>Lifting condensation level</i>	Level at which a parcel of moist air becomes saturated when lifted dry adiabatically
<i>Potential temperature</i>	Temperature that a parcel of dry air would have if brought adiabatically to a standard pressure (i.e., remains constant with pressure changes)
<i>Roughness sublayer</i>	Lowest ABL layer adjacent to land surface and influenced by roughness elements (e.g., trees, buildings, vegetation). Layer depth (or local blending height) is app. 2–5 times the height of roughness elements.
<i>Specific humidity</i>	Mass of water vapor in a unit mass of moist air (i.e., remains constant with pressure changes). May be approximated by the (water vapor) mixing ratio (i.e., mass of water vapor in a unit mass of dry air)
<i>Stable boundary layer [SBL]</i>	Cool stable layer adjacent to the ground characterized by a positive vertical potential temperature gradient developing due to radiative cooling of the land surface during the night (i.e., nocturnal boundary layer [NBL]) or when warm air moves over a cooler surface (e.g., snow or ice). Mixing in the SBL is mainly driven by shear (i.e., mechanical turbulence) and intermittent turbulence events.
<i>Surface layer</i>	Atmospheric layer where mechanical generation of turbulence dominates extending from the top of the roughness sublayer to about 10% of the ABL height

blending height defines the height above which the impact of individual surface patches vanishes and where the ABL can be considered to be homogeneous. Regional blending heights depend on regional (macro-scale) roughness characteristics of the surface patches and are higher than local blending heights, which mainly depend on (microscale) roughness characteristics (e.g., Brutsaert, 1998).

The state of the ABL (e.g., air temperature and humidity, turbulence characteristics) is controlled by the exchange of heat, momentum, and scalars (e.g., water vapor, CO<sub>2</sub>, methane, aerosols) between the land surface and the ABL and between the free troposphere and the ABL (Fig. 4). Diurnal growth of the convective ABL (CBL or mixed layer) causes warmer and typically drier air to be entrained into the ABL from the free troposphere. The land-atmosphere exchange of heat, momentum, and scalars is mediated by the state of the ABL and by the state of the land surface. For example, evapotranspiration and carbon uptake are partly controlled by atmospheric humidity and precipitation and, at the same time, by surface conditions such as vegetation type, vegetation structure, phenology, and soil moisture.

The growth rate of the daytime ABL (or mixed layer) is mostly driven by thermal eddies, and thus depends on available energy at the land surface and how energy is partitioned between latent and sensible heat fluxes, i.e. the Bowen ratio (Fig. 5). If a greater portion of available energy is converted into sensible heat then this leads to a higher Bowen ratio, and the ABL grows more rapidly (Yi et al., 2001), while the opposite is true for a low Bowen ratio (i.e., ABL remains shallower when more energy goes to latent heat). The rate of growth of the mixed layer is also determined by the strength of the capping inversion and subsequent entrainment (Driedonks and Tennekes, 1984; Wyngaard and Brost, 1984), the vertical rate of change of temperature and moisture, and the shear-mixing by wind (Batchvarova and Gryning, 1991). In addition to local drivers of ABL development, synoptic drivers (e.g., frontal circulations of midlatitude cyclones, persistent anticyclones) often induce strong vertical motions and temperature and moisture advection that can substantially alter the state of the ABL (e.g., Schumacher et al., 2019; Sinclair et al., 2010) and result in changes in the strength and

height of the capping inversion (e.g., Mecham et al., 2010). In some cases, subsidence caused by large- or meso-scale circulation can substantially suppress ABL growth and needs to be accounted for when assessing land-atmosphere interactions (e.g., Myrup et al., 1982; Petersen et al., 2015; Rey-Sanchez et al., 2021).

At sunset, when solar heating of the surface ceases, buoyancy-driven turbulent mixing rapidly declines and the onset of the stable nocturnal ABL (NBL) occurs at the surface, leaving a residual layer aloft (Fig. 1). The residual layer can become detached and decoupled from the surface and from the shallow NBL (< 30 m) during periods of very stable atmospheric conditions when vertical mixing is strongly suppressed (e.g., Banta et al., 2007). The decoupling of the surface and the NBL has important implications for the accuracy, representativeness, and interpretation of eddy covariance surface flux measurements, which require sufficient intensity of turbulent mixing for valid measurements of surface fluxes. The NBL is characterized by a strong, shallow temperature inversion caused by surface radiative cooling. In contrast, potential temperature and moisture in the residual layer is well-mixed but turbulence is weak and intermittent. Stable boundary layers (SBL) can also develop during daytime when warmer air moves over cooler land or water surfaces or during the winter in mid to high latitudes, particularly over snow and ice surfaces. Detecting the height of the SBL can be ambiguous (Seibert et al., 2000) due to the multiple processes involved in SBL development such as wind shear-induced turbulence, radiation divergence within the SBL, and orographically induced gravity waves. When turbulence is strongly suppressed in a very stable boundary layer, turbulent energy fluxes may be negligible, and the net radiation at the land surface is solely balanced by the ground heat flux. In contrast, in a weakly stable boundary layer, turbulence can be well-developed. The top of the layer of continuous turbulence is often taken as the height of the SBL. However, due to the ambiguity of defining and detecting the height of a SBL, ensemble approaches based on a range of ABLH definitions under stable conditions may be preferable (e.g., Stiperski et al., 2020) [a more detailed discussion of the physical processes contributing to SBL development is given by Mahrt (1999) and Steeneveld (2014)].

A dynamic understanding of the tight coupling between surface fluxes as measured by the eddy covariance technique (or other techniques such as scintillometry and flux gradients) and growth and decline of the ABL is thus essential to improve the current understanding of the land-atmosphere system and to properly account for dynamic atmospheric processes in studies of land-atmosphere interactions. This may be especially true for the interpretation of nighttime fluxes or fluxes collected under stable atmospheric conditions or in complex terrain (e.g., Kutter et al., 2017; Menke et al., 2019).

## 2.2. Importance of atmospheric boundary layer height for land-atmosphere interactions

The ABL mixing height (ABLH) can be defined as the thickness of the turbulent atmospheric layer adjacent to the ground surface and is an indicator of the volume of air throughout which heat, momentum, and scalars may mix (see Seibert et al., 2000 for a more detailed discussion). During daytime, surface emissions of aerosols, water vapor, and trace gases are mixed throughout the ABL by convective and mechanical turbulence on a time scale from typically 20–30 minutes to a few hours (i.e., CBL), while mixing can be substantially reduced in the SBL (e.g., Gult et al., 1997; Seibert et al., 2000; Yi et al., 2000; Yi et al., 2001). The CBL is capped by an entrainment layer where the sign of the heat flux gradient reverses (i.e., sensible heat is entrained into the CBL), while the SBL usually consists of a lower layer of continuous turbulence topped by a layer of sporadic or intermittent turbulence.

The ABLH is a critical variable for understanding and constraining ecosystem and climate dynamics. For example, air pollutants in deep ABLs are well mixed, leading to lower pollutant concentrations, while shallow SBL favor accumulation of pollutants to higher concentrations (e.g., Yin et al., 2019). Carbon dioxide concentrations in the ABL are governed by large diel variations in ABLH (Yi et al., 2001), changing signs of CO<sub>2</sub> surface fluxes, and daily and seasonal variations in the differences between free troposphere and ABL CO<sub>2</sub> concentrations (Davis et al., 2003; Yi et al., 2004; Vila-Guerau de Arellano et al., 2004). Given that ABLH controls the volume that is subject to mixing, differences in CO<sub>2</sub> concentrations between the ABL and free troposphere covary with ABLH on diurnal and seasonal timescales – also known as the rectifier effect (e.g., Denning et al., 1995). This effect (Denning et al., 1999; Yi et al., 2004) and the simple relationship between ABLH and ABL CO<sub>2</sub> concentrations (Díaz-Isaac et al., 2018) have direct implications for

atmospheric CO<sub>2</sub> transport and its representation in atmospheric transport models (Feng et al., 2020).

The ABLH also directly affects the heat capacity of the ABL and therefore its potential to slow or enhance daily atmospheric warming rates (e.g., Panwar et al., 2019). ABL heights also play a crucial role for the onset of precipitation events and cloud dynamics (e.g., Juang et al., 2007b; Siqueira et al., 2009; Konings et al., 2010; Yin et al., 2015). Convective clouds and locally generated precipitation only develop once the top of the ABL reaches the lifting condensation level (LCL, defined by the height where a parcel of moist air – lifted dry adiabatically from the surface – reaches saturation, see Fig. 6). However, the relationship between LCL and ABLH is only a first-order criterion (Yin et al., 2015) and boundary layer cloud development is additionally governed by other complex feedback mechanisms between temperature and humidity dynamics and cloud development (see Betts, 1973 and van Stratum et al., 2014 for detailed discussions). The transition from clear to cloudy ABLs has important implications for ABL dynamics. Cloud-ABL feedbacks lead to a reduction in ABL growth rate and drying of the sub-cloud layer, which is caused by enhanced entrainment and by moisture transport to the cloud layer (van Stratum et al., 2014). Convective cloud and precipitation development and deep convection will lead to deviations from the ABL behavior described above. For example, gust fronts associated with convective downdrafts quickly alter ABL state and consequently affect surface fluxes (e.g., Grant and van den Heever, 2016). Transitions from daytime CBLs to nighttime SBLs (see Angevine et al., 2020) and from clear sky to cloudy conditions also remain areas of current research (see van Stratum et al., 2014).

## 2.3. Measurements of atmospheric boundary layer heights

Traditionally, ABLH has been derived from atmospheric profiles of air temperature and humidity measured by radiosondes. Such profile measurements are labor-intensive and are thus often made only a couple of times per day or are limited to short-term intensive field campaigns (e.g., Salcido et al., 2020). Operational soundings (e.g., national weather service soundings) are synchronized to noon and midnight Coordinated Universal Time (UTC), not local time, and sample different parts of daily ABL development (Fig. 1) depending on latitude and longitude. Recent progress in atmospheric observation techniques, specifically radar profilers and lidar-based devices, now allow us to continuously measure ABLH, automatically and at high temporal resolution. Instruments

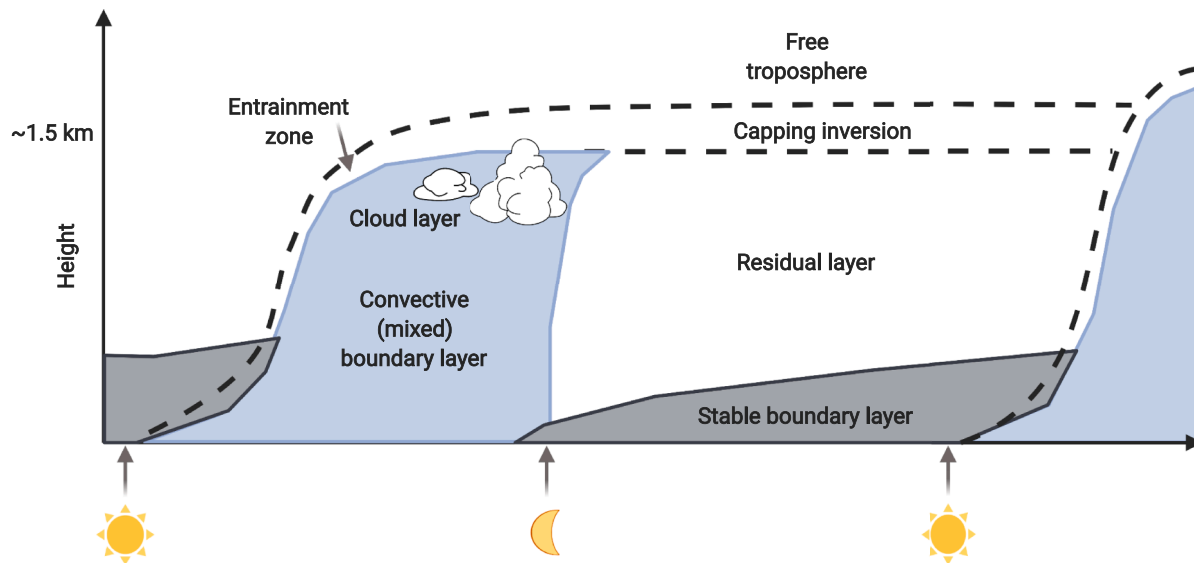


**Fig. 1.** Ideal diurnal development of the atmospheric boundary layer (ABL) during the day, from sunrise to sunset, and transformation to the stable (nocturnal) boundary layer from sunset to sunrise (figure after Stull, 1988).

capable of such measurements are commercially available, relatively affordable, require minimal maintenance, and are suited to deployment even at remote field sites such as those typical of the FLUXNET network. However, at present, direct ABL measurements are only made at a small fraction of sites (see Tab. 2 for a list of sites) and ABL data are typically not submitted to FLUXNET or the regional flux networks.

### 3. Currently available technology for atmospheric boundary layer observations

Various ground-based technologies are available for observations of aerodynamic and thermodynamic (i.e., air temperature and humidity) ABL properties (Table 2, e.g., Wilczak et al., 1996; Seibert et al., 2000; Emeis et al., 2004). Here, we outline basic measurement principles of (1) radiosonde observations, (2) ceilometers and aerosol backscatter lidars, (3) Doppler sodar, and (4) wind profiling radars and lidars. Differences in measurement techniques and their observed variables can lead to discrepancies between ABLH estimates, which typically are in the order

of 10% (for well defined capping inversion) to 25% (for weak capping inversions or non-well mixed ABL) for CBLs while being much more variable for SBLs. For a detailed discussion of technique-dependent differences in ABLH estimates, the readers are referred to Seibert et al. (2000).

#### 3.1. Radiosonde observations

Radiosonde observations have been widely used for decades to detect ABLH (e.g., Barr and Betts, 1997; Yi et al., 2001; Wang and Wang, 2014; Wouters et al., 2019; Salcido et al., 2020). Atmospheric profiles from radiosonde observations provide detailed information on the vertical variation of air temperature and humidity, air pressure, and wind speed and direction. During the daytime, the upper boundary of the ABL can be defined as the height where the maximum (i.e., positive) vertical gradient in potential temperature is located, coinciding with a sharp increase in potential temperature, or as the height where the minimum (i.e., negative) vertical gradient of specific humidity is observed,

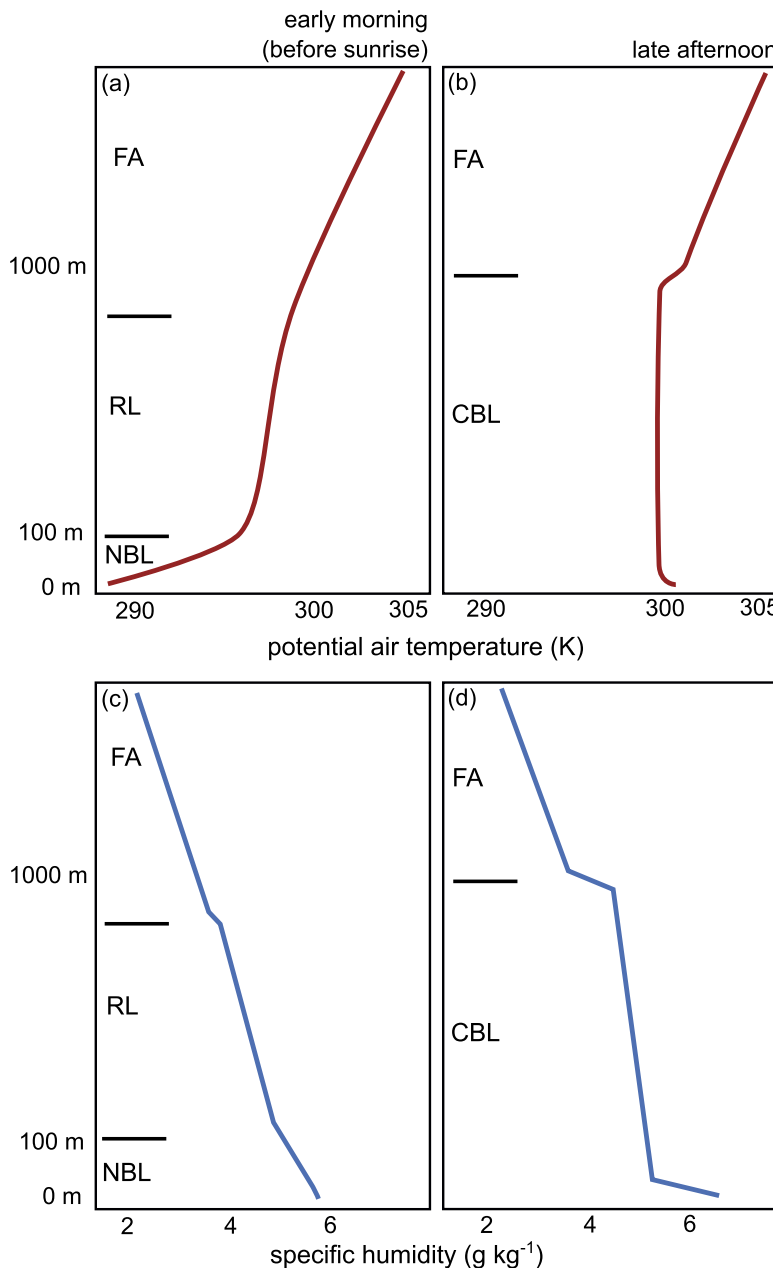


**Fig. 2.** Typical atmospheric boundary layer profiles of (a and b) potential temperature and (c and d) specific humidity (a and c) in the early morning just before sunrise and (b and d) in the late afternoon. Examples typical for boreal forests are shown (see Barr and Betts 1997). Diurnal changes in atmospheric boundary layer structure are shown to the left of the profiles (FA = free atmosphere, RL = residual layer, NBL = nocturnal boundary layer, CBL = convective boundary layer). Figure adapted from Stull (1988).

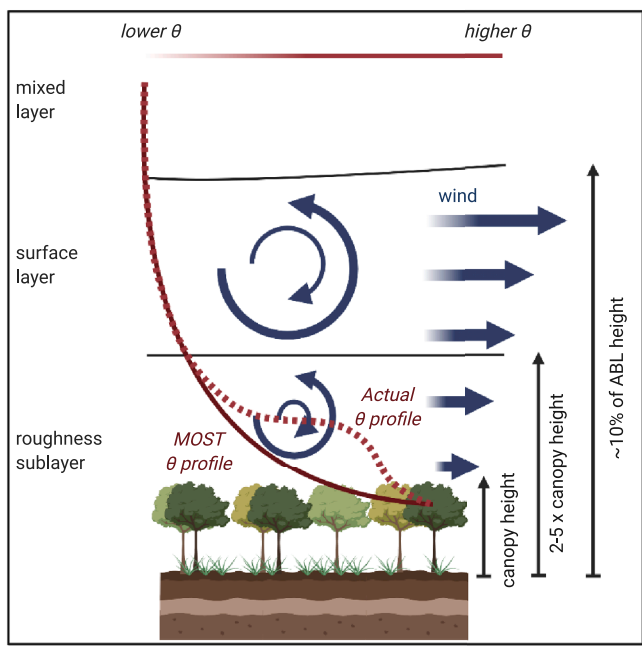
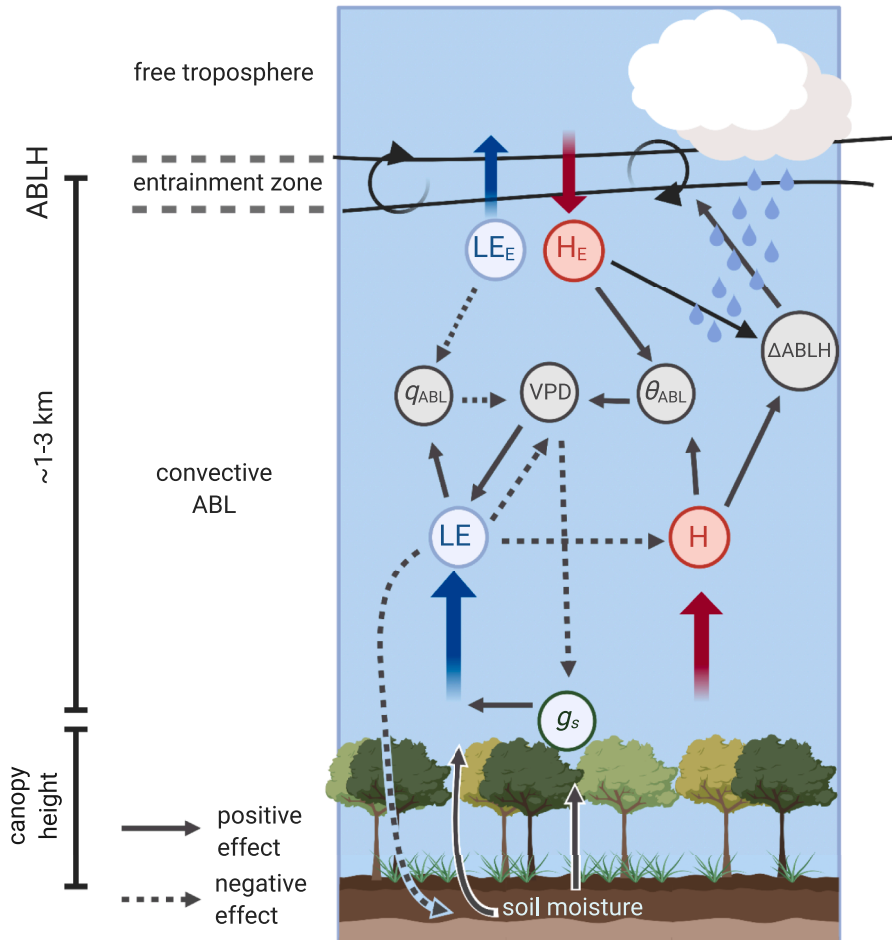


**Fig. 3.** Typical structure of the lower atmospheric boundary layer above an extended homogeneous surface with actual potential temperature ( $\theta$ ) profile and  $\theta$  profile according to Monin-Obukhov similarity theory. Horizontal arrows indicate mean wind speed profile (adapted from Novick and Katul, 2020).



coinciding with a sharp drop in specific humidity (Wang and Wang, 2014, Fig. 2 and 7). However, defining ABLH during stable atmospheric conditions using air temperature, humidity, and wind profiles is challenging since no universal relationships exist to determine NBL and SBL heights (Seibert et al., 2000). With a 1 s temporal and ~5 m vertical resolution, the resolution of radiosonde observations is usually similar to the resolution of ceilometers and lidars (<30 m) but varies with atmospheric conditions and ascent speed of the sonde. Balloons are often used to launch radiosondes and travel horizontally with the mean wind. Depending on wind conditions, the location of the derived ABLH may no longer be representative of the conditions at the launch location. Radiosonde observations represent the most labor-intensive way of measuring ABLH requiring ongoing costs for manual labor and instrumentation. Global networks of synoptic observation sites provide daily radiosonde data, which are archived in the Integrated Global Radiosonde Archive (Durre et al., 2006; available through the NOAA National Centers for Environmental Information) and in the University of Wyoming sounding data archive (<http://weather.uwyo.edu/upperair/sounding.html>). However, the launch points for long-term observations are fixed and may not represent the air masses surrounding flux tower sites. Relatively low-cost, lightweight ABL-focused radiosondes (i.e., Windsond weather balloon systems; Bessardon et al., 2019) have recently emerged that allow to increase temporal and spatial resolution of sampling (see Table 2).

### 3.2. Ceilometers and lidars

Ceilometers and aerosol backscatter lidars emit a laser pulse at wavelengths between 300 and 1500 nm, which is scattered in the

**Fig. 4.** Daytime interactions and feedbacks between surface sensible (H) and latent heat (LE) fluxes, entrainment fluxes ( $H_E$ ,  $LE_E$ ), atmospheric boundary layer growth rate ( $\Delta ABLH$ ), land surface (e.g., soil moisture) and vegetation conditions (e.g., stomatal conductance [ $g_s$ ]), and state of the atmospheric boundary layer (i.e., vapor pressure deficit [VPD], mixed-layer potential temperature [ $\theta_{ABL}$ ], and mixed-layer specific humidity [ $q_{ABL}$ ])). The ABL top separates the convective ABL from the free troposphere. This separation zone is defined as the atmospheric boundary layer height (ABLH). Note that ABLH is not constant in time, and that horizontal advection (not shown) will also impact ABL quantities.

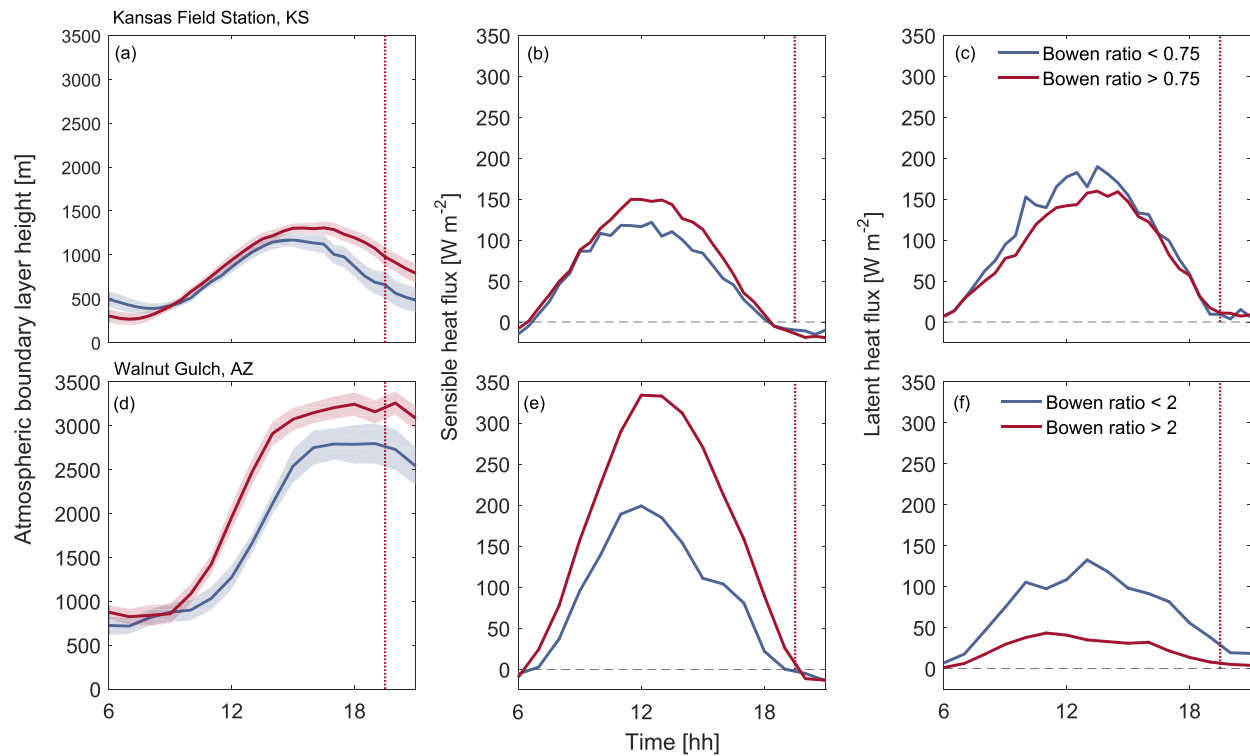


**Fig. 5.** (a) Mean diurnal development of the atmospheric boundary layer height (ABLH) in July 2017 at the Kansas Field Station flux tower site (US-KFS) on days with low Bowen ratio ( $<0.75$ ) and high Bowen ratio ( $>0.75$ ) and mean diurnal variation of (b) sensible and (c) latent heat fluxes on days with low and high Bowen ratio. (d) Mean diurnal development of ABLH between July and September 2019 at the Walnut Gulch flux tower site (US-Wkg/Whs) on days with low Bowen ratio ( $<2$ ) and high Bowen ratio ( $>2$ ) and mean diurnal variation of (e) sensible and (f) latent heat fluxes on days with low and high Bowen ratio at the same site. Vertical red dotted lines indicate the approximate timing of sunset. Atmospheric boundary layer heights were derived from aerosol backscatter profiles measured by ceilometers. Note that the detected early morning ABLH might be the top of the residual layer.

atmosphere by aerosols. A portion of this scatter is directed back to the receiver and recorded as backscatter. Ceilometer is a term more traditionally used to describe aerosol backscatter lidars that are used to detect the height of the cloud base, while backscatter lidar is a more general term. Aerosol backscatter lidars, including those called ceilometers, produce aerosol profiles for each laser pulse, which can be used to derive cloud base height and, if the signal to noise of the instrument is sufficient, ABLH (Kotthaus and Grimmond, 2018a; Lotterer and Piringer, 2016). The ABLH in this case is typically defined as the height at which aerosol concentration and thus the backscatter signal decreases sharply (Fig. 8). Therefore, the ability of an aerosol backscatter lidar to detect ABLH depends on the level of aerosol concentrations in the ABL and on the sensitivity of the instrument to low aerosol concentrations (e.g., Eresmaa et al., 2006). In clean air, retrievals of ABLH may therefore be problematic with lower signal-to-noise backscatter lidars.

Strong vertical gradients of attenuated backscatter often coincide with the location of the capping inversion, but considerable differences can occur, such as during the evening transition when new gradients of backscatter slowly form after the turbulence has decayed (Kotthaus et al., 2018). Additionally, interpreting aerosol backscatter profiles can be difficult if aerosol layers are the result of advection processes or if vertical aerosol gradients are weak such as in some SBLs. In contrast to the ABLH derivation from thermodynamic profiles using radiosondes, aerosol backscatter lidars allow more direct observations of the depth of the mixing layer. Differences in these ABLH estimates can be caused by turbulence (and mixing) extending beyond the capping inversion (Seibert et al., 2000).

The advantage of the aerosol backscatter lidar is that it allows continuous observations of ABLH and that it can be a relatively inexpensive instrument (Table 2). Additionally, aerosol backscatter lidars

provide information on the height of cloud base above the ground (see Fig. 6), and considerable effort has gone into the development of automated algorithms for determining ABLH (e.g., Davis et al., 2000; Brooks, 2003). In contrast to radiosonde observations, aerosol backscatter lidars do not measure atmospheric profiles of temperature and humidity and thus do not allow the derivation of potential temperature and specific humidity gradients in the free troposphere. However, these gradients are essential for the calculation of entrainment fluxes (van Heerwaarden et al., 2009).

To add information on atmospheric humidity profiles, aerosol backscatter lidars can be paired with radiosonde observations or with water vapor lidar instruments (e.g., compact water vapor differential absorption lidar [DIAL], Newsom et al., 2020; Raman lidar, Wulfmeyer et al., 2018), which allow continuous measurements of water vapor profiles up to a few kilometers above ground (Fig. 9). Alternatively, passive detection of atmospheric emission and absorption lines in the infrared and microwave bands can also provide information on temperature and humidity gradients (e.g., Löhnert et al., 2009). Microwave and infrared radiometers use variations in water vapor and oxygen emissions with pressure at selected wavelengths to deduce profiles of temperature, humidity, and cloud liquid water or to measure column integrated water vapor and liquid water. The observed variations are very subtle requiring careful calibration. Some studies report success at resolving simple shallow ABLs of the order of 100 meters, although caution should be exercised in interpreting measurements of deeper or more complex ABLs since the vertical resolution can degrade significantly (e.g., Blumberg et al., 2015). The Global Energy and Water Exchanges (GEWEX) Land-Atmosphere Feedback Observatory (GLAFO) initiative aims to pair soil and ecosystem observations with lidars and profiling systems across different climate regions to give new insights

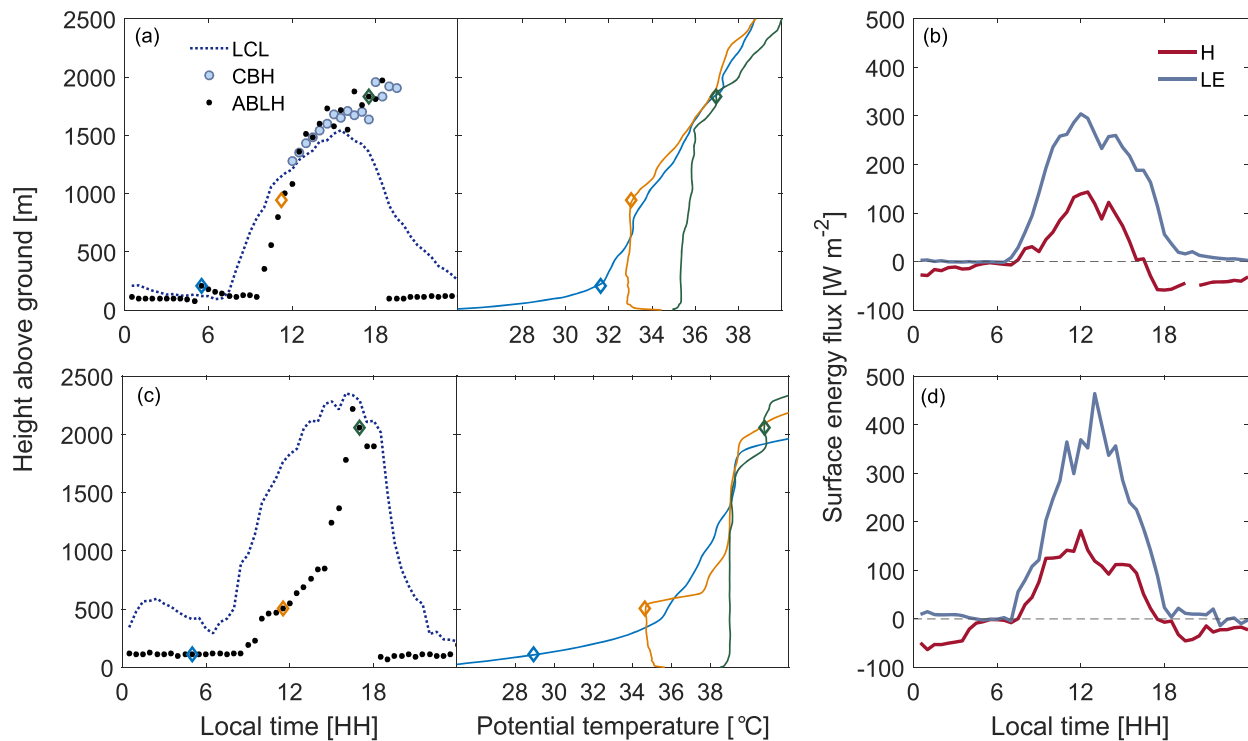


**Fig. 6.** Diurnal growth of the atmospheric boundary layer (ABL) at the Southern Great Plains atmospheric observatory in Oklahoma, U.S.A. (US-ARM) on (a) 16 September 2018 [day with ABL cloud development] and on (c) 6 September 2019 [clear-sky day] and concurrent changes in lifting condensation level (LCL, blue dotted line) and, if present, in cloud base height (CBH, blue circles, if below 2,500 m above ground) as detected by Vaisala CL-31 ceilometer measurements. ABL heights (ABLH, black dots) were defined as the top of the mixed layer as detected by ceilometer measurements. Solid blue, yellow, and green lines show radiosonde observation of potential temperature profiles at 05:00, 11:30, and 17:00h, respectively. Diamonds show ABLH as derived from ceilometer measurements at the radiosonde launch times. (b,d) Sensible (H) and latent heat (LE) fluxes for the same days measured using the eddy covariance technique at the same site.

into complex feedback mechanisms between land and atmosphere and opens new opportunities for collaboration between FLUXNET scientists and atmospheric scientists (Wulfmeyer et al., 2020).

New active ground-based remote-sensing technologies, such as Doppler, Raman, and DIAL lidar are already or will soon become commercially available (Wulfmeyer et al., 2018). They offer the possibility for quasi-continuous thermodynamic profiles of the entire ABL at unprecedented accuracy and spatio-temporal resolution (Wulfmeyer et al., 2015) adding crucial information on the state of the ABL to continuous ABLH measurements. These instruments even allow to measure turbulent fluxes of sensible and latent heat between the surface layer and the entrainment zone directly, via eddy-covariance from remotely sensed data (Behrendt et al., 2020). Such measurements allow ABLH detection as the height at which the sensible heat flux changes its sign. The potential of such observations was explored at the Yatir forest FLUXNET site (IL-Yat). As part of a study on land-atmosphere feedbacks, two Doppler lidars and a ceilometer were deployed in order to investigate the impact of heterogeneity-induced secondary circulations on the surface flux measurements (Eder et al. 2015b) and the effect of this distinct surface heterogeneity on the structure and dynamics of the ABL (Brugger et al. 2018). To give new insights into complex feedback mechanisms between land and atmosphere, the GEWEX Land-Atmosphere Feedback Observatory (GLAFO) initiative aims to pair soil and ecosystem observations with lidars and profiling systems across a wide range of climate regions (Wulfmeyer et al., 2020). The initiative opens new opportunities for collaboration bringing together the expertise of ecosystem and atmospheric scientists.

### 3.3. Doppler sodar

A Doppler sodar is an acoustic remote sensing instrument. Doppler sodars derive atmospheric profiles of horizontal and vertical wind velocities and temperature (when combined with a radio acoustic sounding system [RASS]) from the scattering of sound pulses (wavelength between 0.1 m and 0.2 m) by atmospheric turbulence (i.e., reflectivity). Vertical reflectivity profiles can be used to derive ABLH since the interface between ABL and free troposphere (i.e., the entrainment zone) is characterized by intense thermodynamic fluctuations and thus by a maximum in reflectivity (Beyrich, 1997). However, the vertical range of sodar instruments is typically restricted to heights well below 1000 m. Deep ABLs can therefore not be detected using sodar technology. Additional constraints of sodar instruments are related to instrument noise issues affecting the local community.

### 3.4. Wind profiling radars and lidars

Another technology widely used to observe the ABL are wind profiling radars (e.g., Yi et al., 2001) and lidars (e.g., Tucker et al., 2009). Wind profiling radars emit pulses of electromagnetic radiation (wavelength of  $\sim 0.5$  m) along one vertical beam and two to four oblique beams, and receive backscatter signals, which can be used to derive atmospheric profiles of wind speed and direction. Radar wind profilers have a wider vertical range than Doppler sodar systems but typically lack coverage at heights below 100 m in the case of the 915 MHz profiler, and below 500 m when using the 449 MHz profiler (Table 2). ABLH can be derived by identifying the maximum signal-to-noise ratio (SNR) in the backscatter, which is proportional to the maximum in the refractive-index structure parameter (Wesely, 1976; White et al., 1991).

**Table 2**

Available technologies for ground-based atmospheric boundary layer observations and specifications of different instrumentation. Specifications and basic information on instruments have been sourced from manufacturer websites. For more details see Tab. S1.

Instruments	Price range*	Wavelength	Power	Vertical Range	Vertical Res.	Weight	Example instrumentation	Basic information
Aerosol backscatter LiDAR (incl. ceilometer)	\$\$	355-1550 nm	20 W - 800 W	7-15 km	5-30 m	10 – 70 kg	Campbell CS135, Lufft CHM 15k NIMBUS, PSI Compact Ceilometer, Vaisala CL51 and CL31 Ceilometers, Micro Pulse LiDAR	Allows cloud base detection and aerosol concentration measurements, vertical profiles of aerosol backscatter are used to determine ABL height
Balloon Sounding	\$ (receiving station \$-\$ \$\$)	-	-	8 – 40 km	variable	10 – 300 g	Windsond, Vaisala RS41, Lockheed Martin LMS-06, GRAW DFM-09, InterMet iMet-1	Radiosondes report wind, temperature, and humidity profiles; ABL height can be derived from profile measurements, measure vertical gradients of temperature and humidity in the free troposphere
Doppler Sodar	\$\$ - \$\$\$	0.1-0.2 m	60-250 W	10-1,000 m	5-50 m	50-100 kg	Metek DSDPA.90-24 and PCS2000, Remtek PA-XS and PA-0, Scintec MFAS	Measures vertical wind profiles and (virtual) temperature profiles with RASS extension
Radar Wind Profiler	\$\$\$\$-\$\$\$\$\$	0.33 – 0.7 m	100 W (average) - 2000 W (max)	2-10 km	Low:60 - 100High: 250 - 500 m	Up to 1,000 kg	Scintec LAP3000 and LAP8000, Radiometrics Raptor	Use electromagnetic radiation pulses to measure wind and precipitation profiles
Lidar Wind Profiler	Profiling lidar: \$\$\$; Scanning lidar: \$\$\$; Raman lidar: \$\$\$\$	1,500 – 2,000 nm	20 - 10,000 W	300 m - 15 km	1 – 150 m	45 kg – 1,630 kg	<i>Profiling lidar:</i> ZephIR300, Leosphere WindCube v2, Spider, Metek Wind Scout, Vaisala Differential Absorption Lidar [DIAL]; <i>Scanning lidar:</i> WindTracer (Lockheed Martin), HALO Photonics Streamline Wind Lidar, Leosphere WindCube 100S and 200S Wind Lidar, NOAA High-Resolution Doppler Lidar, Purple Pulse Raman Lidar, Raymetrics Raman Lidar	Lidar wind profilers allow for tracking of moving objects (e.g., aerosols) and a depiction of wind fields along a narrow cone around zenith (profiling) or for varying angles (scanning). Raman Lidar and DIAL allow continuous observations of temperature and humidity profiles.

\* Price range is estimated based on current instrument pricing in the respective instrument classes (\$ < 10k USD, \$\$ 10k-50k USD, \$\$\$ 50k-100k USD, \$\$\$\$ 100k-500k USD, \$\$\$\$\$ > 500k USD).

This maximum SNR typically coincides with lower humidity levels (White et al., 1991; Grimsdell and Angevine, 1998), buoyancy fluctuations (Angevine et al., 1994; Bianco et al., 2008), and the steepest gradient in air temperature, humidity, and aerosol concentration at the transition between ABL and free troposphere (Compton et al., 2013; Molod et al., 2015). A continuous time series of ABLH can be obtained after careful processing of the profiler data (e.g., Bianco et al., 2008; Molod et al., 2015).

Wind profiling lidars have a more powerful and spectrally narrower laser light source than ceilometers and are similar to radars except that they use light ( $\sim 0.5$  -  $2 \mu\text{m}$ ) instead of radio waves ( $\sim 0.5$  m). Due to the use of shorter wavelengths, wind profiling lidars can track the movement of aerosols with air motions within the scanning cone to estimate wind speed and direction (Grund et al., 2001). A combination of backscatter and atmospheric turbulence data can be used to derive ABLH (Tucker et al., 2009). Wind profiling lidars can be designed with high vertical resolution and some can be pointed at an angle to resolve shallow nighttime ABLH as well as resolve daytime ABLs (e.g., Tucker et al. 2009). The ability to measure atmospheric turbulence also yields perhaps the most direct measure of the active mixing depth of the ABL (Tucker et al., 2009). Further, wind profiling lidar can be co-located with DIAL to measure eddy covariance flux profiles of water vapor (Kiemle et al., 2007) and potentially of CO<sub>2</sub> as instrumentation improves (Gibert et al., 2011).

#### 4. Atmospheric boundary layer observations co-located with eddy covariance flux instrumentation

To date, there have been relatively few instances of continuous, high-frequency atmospheric measurements of ABLH being conducted simultaneously with co-located eddy covariance flux measurements (Tab. 3) and ABLH observations are not routinely shared through FLUXNET or the regional observation networks. Until 2006, when a ceilometer was installed at the Morgan Monroe State Forest site, it appears that previous efforts had been limited to campaigns of only a few months to one year in duration. For example, in 1998 a wind profiling radar and radiosonde observation system was deployed for one year at the WLEF tall tower (US-PFa; Yi et al., 2001; 2004) and for a second year, in 1999, at the Walker Branch Watershed (US-WBW). The Park Falls flux tower included a co-located ceilometer for several years, but it was removed around 2005. The Morgan Monroe measurements were discontinued in 2013.

Currently, there are ongoing, long-term ABLH measurements at (or near) a few sites in North America (see Tab. 3 for site information). Measurements at the Southern Great Plains (US-ARM), the Oliktok Point (US-A03), and the Utqiagvik (US-A10) sites are collected as part of the Department of Energy Atmospheric Radiation Measurement program ([www.arm.gov](http://www.arm.gov)), while the Twitchell Island (US-Twt1 and US-Tw3) measurements are collected through the NOAA ESRL program. The measurements at Howland Forest (US-Ho1) were initiated by the site PI, while those at Walnut Gulch (US-Wkg) and Kansas Field Station (US-KFS) were initiated by site collaborators. Campaigns on NBLs were

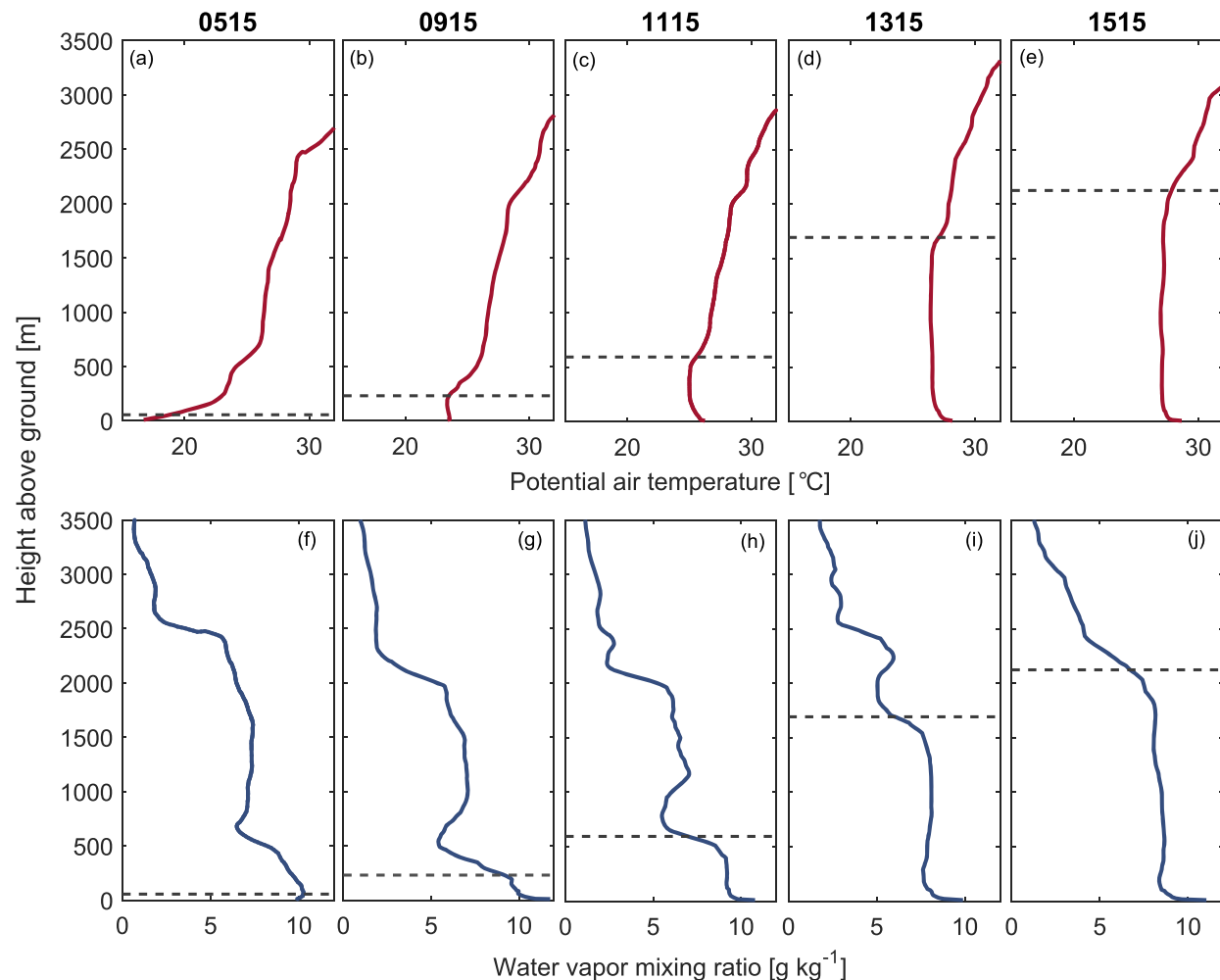


**Fig. 7.** Atmospheric profiles of (a-e) potential temperature and (f-j) water vapor mixing ratio between 05:15h and 15:15h local time on 30 July 1996 at Candle Lake, Saskatchewan, Canada (data from the BOREAS Southern Study Area: [https://daac.ornl.gov/cgi-bin/dsviewer.pl?ds\\_id=238](https://daac.ornl.gov/cgi-bin/dsviewer.pl?ds_id=238)). Dashed lines show height of the atmospheric boundary layer/mixing layer as determined by the gradient method (see Seidel et al., 2010).

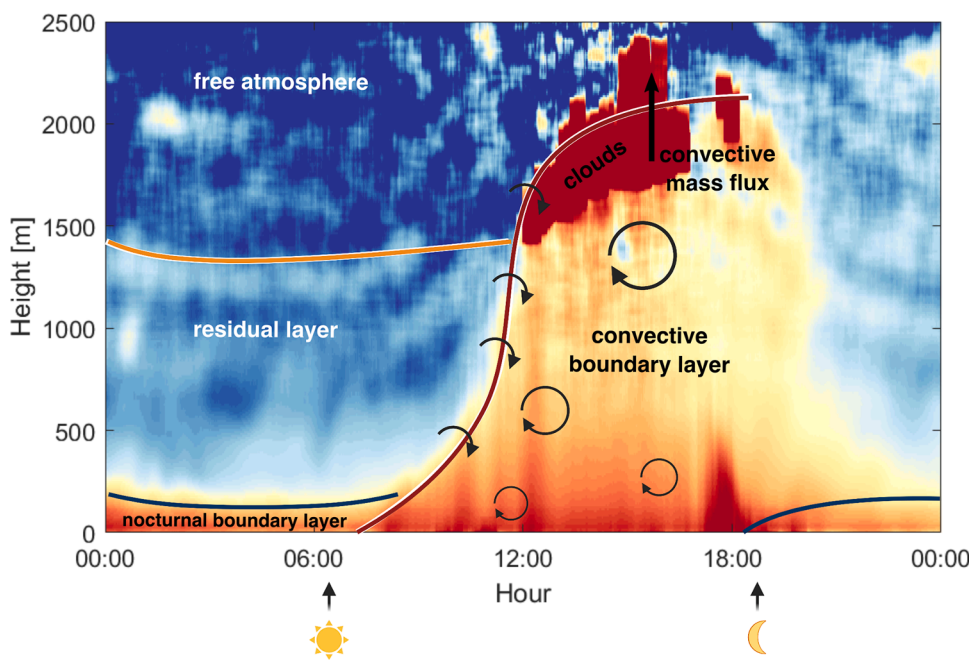


**Fig. 8.** Example of the diurnal development of a backscatter profile at the Southern Great Plains atmospheric observatory in Oklahoma, U.S.A.. Colors show a full day of the logarithm of smoothed attenuated backscatter in arbitrary units (red = high aerosol backscatter, blue = low aerosol backscatter). Backscatter measurements were conducted using a Vaisala CL-31 ceilometer. Lines indicate estimates of the location of the top of the nocturnal boundary layer, residual layer, and convective boundary layer. Boundary layer cloud development starts at around noon initiating convective mass flux. Timing of sunrise and sunset are shown too.

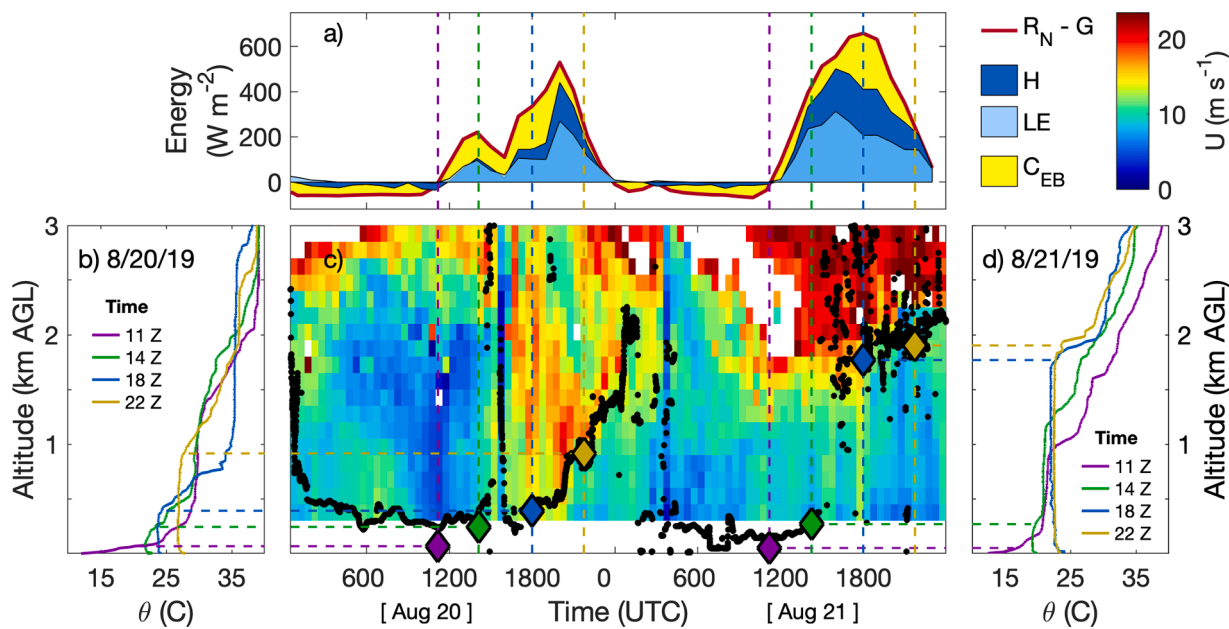


**Fig. 9.** (a) Cumulative (i.e., stacked) latent, sensible heat flux, and energy balance residual (LE, H, and C<sub>EB</sub>) measured by Ameriflux tower US-PFa at 30 m AGL with mean net radiation and ground flux (R<sub>N</sub> and G) measurements from 17 nearby eddy-covariance towers installed during the CHEESEHEAD19 field campaign; (b) and (d) daytime radiosonde profiles on August 20 and 21, 2019; and (c) winds measured by a 449 MHz radar wind profiler overlaid with Vaisala CL51 ceilometer (black circles) and radiosonde-derived (diamonds) ABL heights ((NCAR/EOL In-situ Sensing Facility 2020); (Butterworth et al., 2021).

conducted at the Tonzi (US-Ton) and Wind River (US-WRC) sites (Wharton et al., 2017). At the 47 National Ecological Observatory Network (NEON) terrestrial sites, neither ceilometers nor wind profilers are included in the instrument package deployed.

In Europe, the Integrated Carbon Observation System (ICOS) network is planning to deploy ceilometers at all Class 1 atmospheric monitoring stations, which are co-located with Ecosystem stations (i.e., eddy covariance flux towers). At the ICOS Sweden Atmosphere sites at Hyltemossa (SE-HTM), Norunda (SE-NOR), and Svartholma (SE-SVH) ceilometers are already in operation and co-located with simultaneous eddy covariance flux measurements. Three sites of the Terrestrial Environmental Observatories (TERENO) pre-Alpine observatory in Germany are equipped with ceilometers for ABLH detection since 2012 (sites DE-Fen, DE-RbW, and DE-Gwg; Eder et al., 2015a; Kiese et al., 2018). The Indianapolis Flux Experiment (INFLUX; Davis et al., 2017), which was running from 2013 through 2017, included eddy covariance flux towers and a Doppler lidar. Co-located surface flux and ABL observation datasets are publicly available only for a few sites. Making more existing observation datasets available to the wider community through public data repositories would enable studies addressing new emerging research questions.

## 5. Research opportunities emerging from co-located ABL and tower-based surface flux observations

Extending current ABL observations across the FLUXNET network would open new opportunities to tackle pressing research questions and add value and exposure to ongoing eddy covariance surface flux measurements (see Table 4 for a summary of possible applications). In this section, we outline how continuous and long-term ABL observations at flux tower sites would provide crucial information to (1) interpret surface flux dynamics at flux tower sites, (2) support flux footprint modelling and quality control of flux measurements (including flux correction algorithms), (3) support regional-scale modelling and upscaling of surface fluxes, (4) and quantify land-atmosphere coupling and validate its representation in Earth system models. Long-term continuous ABL observations have the advantage that they can capture ABL responses to seasonal changes in surface fluxes (Bianco et al.,

2011) and to interannual variability of surface and boundary-layer dynamic conditions (e.g., drought, Miralles et al., 2014). However, cost limitation or requirement of personnel often only allow long-term observations of a limited range of atmospheric variables (e.g., ABLH). Shorter intense ABL observation campaigns (e.g., BOREAS, FIFE, LAFE) typically feature a wider range of observed atmospheric variables but are only feasible at a few selected sites (Barr and Betts, 1997; Betts, 1992; Wulfmeyer et al., 2018).

For site-specific applications in heterogeneous terrain, spatial mismatch between surface flux footprints and ABL source areas should be carefully assessed to ensure that observed fluxes are representative of the observed ABL conditions (e.g., Sugita et al., 1997; Wang et al., 2006). Horizontal scales of surface flux footprints from flux towers can be substantially smaller than source areas of meteorological observations in the ABL, particularly for deep ABLs (Wilson and Swaters, 1991; Schmid, 1994). Scintillometers allow measurements of area-averaged surface sensible heat and momentum fluxes over a path length of up to several kilometers and can be paired with eddy covariance flux measurements (see Meijninger et al., 2002). Comparisons of ecosystem-scale surface fluxes from eddy covariance towers and landscape-scale area-averaged surface fluxes from scintillometers can help assess the representativeness of flux tower measurements for larger scale ABL development.

### 5.1. Interpretation of surface flux measurements

**To fully understand the feedback between surface fluxes and the atmosphere, we require ABLH observations in addition to eddy covariance flux measurements.** Fluxes of mass and energy at the land surface, as measured at eddy covariance tower sites, are not isolated from the conditions of ABL and free troposphere. Mass and energy fluxes at the land surface respond to changes in ABLH and to the heat, moisture, and matter that is mixed into the growing ABL from the free troposphere (i.e., entrainment). In turn, the depth of the ABL and the concentration of scalars within it are a function of the surface fluxes and the entrainment of dry air from above the growing ABL (Denmead et al., 1996; Davis et al., 1997). Thus, observations of ABLH and of its growth can support the interpretation of surface flux observations.

**Table 3**

Examples of previous and ongoing atmospheric boundary layer observations co-located with eddy covariance flux towers. Links to publications and additional information on the flux tower sites can be accessed through the footnotes. Ecosystem types include deciduous broadleaf forest (DBF), mixed forest (MF), evergreen needleleaf forest (ENF), cropland (CRO), barren sparse vegetation (BSV), woody savanna (WSA), urban (URB), grassland (GRA), open shrubland (OSH), and evergreen broadleaf forest (EBF).

Location	Site Code	Contact	Ecosystem	Measurements	Period	Instrument(s)
Walker Branch, TN <sub>1</sub>	US-WBW	K. Davis and D. Baldocchi	DBF	boundary layer height, wind profiles, radar reflectivity, thermodynamics	1999	NCAR Integrated Sounding System
Park Falls, WI <sub>1</sub>	US-PFa	K. Davis	MF	boundary layer height, wind profiles, radar reflectivity cloud base and fraction, thermodynamics	1998, 1999	NCAR Integrated Sounding System
Old Jack Pine, SK (BOREAS) <sub>2</sub>	CA-Ojp	J. Wilczak	ENF	boundary layer height	1994	NOAA/ETL 915 MHz radar wind/RASS profiler
Morgan Monroe State Forest, IN <sub>3</sub>	US-MMS	K. Novick	DBF	boundary layer height, cloud base and amount; backscatter profile	2006-2009, 2011-2013	Vaisala CL31 lidar ceilometer
Southern Great Plains ARM, OK <sub>4</sub>	US-ARM	S. Biraud	CRO	boundary layer height, cloud base and amount; backscatter profile; wind profiles	2011-	CEIL lidar ceilometer; radar wind profiler; micropulse lidar
Utqiagvik, AK <sub>5</sub>	US-A10	R. Sullivan	BSV	boundary layer height, cloud base and amount, water vapor, temperature, and turbulence profiles	2011-	Ceilometer, micropulse lidar, balloon sonde, G-band radiometer profiler, microwave radiometer
Tonzi, CA <sub>6</sub>	US-Ton	S. Wharton and D. Baldocchi	WSA	wind profile from ground to 150m, thermodynamic and wind profiles from ground to top of troposphere, ABL height	2012, 2013	WindCube v2, ZephIR 300, radiosondes
Wind River, WA <sub>7</sub>	US-Wrc	S. Wharton	ENF	Wind profile from ground to 150m, thermodynamic and wind profiles from ground to top of troposphere, ABL height	2012	WindCube v2, radiosondes
Howland Forest, ME <sub>8</sub>	US-Ho1	D. Hollinger	ENF	boundary layer height, cloud base and amount; backscatter profile	2013-	Vaisala CL31 lidar ceilometer
INFLUX (Indianapolis Flux Experiment) <sub>9</sub>	-	K. Davis and A. Brewer	URB	boundary layer height, wind profiles, turbulence profiles, cloud base and fraction	2013-2017	HALO Photonics scanning doppler lidar
Oliktok Point, AK <sub>5</sub>	US-A03	R. Sullivan	BSV	boundary layer height, cloud base and amount, water vapor, temperature, and turbulence profiles	2014-	Ceilometer, micropulse lidar, balloon sonde, radar wind profiler, Doppler lidar
Walnut Gulch, AZ <sub>10,11</sub>	US-Wkg/ Whs	J. Perkins and P. Hazenberg	GRA/OSH	boundary layer height, cloud base and amount; backscatter profile	2017-	Lufft CHM15k lidar ceilometer
Walnut Gulch, AZ <sub>10,11</sub>	US-Wkg/ Whs	A. Richardson	GRA/OSH	boundary layer height, cloud base and amount; backscatter profile	2019-	Campbell CS135 lidar ceilometer
CHEESEHEAD19, WI <sub>12</sub>	US-PFa	A. Desai	various	boundary layer height, cloud base, aerosol backscatter and polarization, PBL temperature, wind and moisture profiles, radar reflectivity, precipitation imaging	June-Oct 2019	NCAR Integrated Sounding System, UW SSEC SPARC (AERI AND HSRL), KIT IFU H2O and wind LiDAR, NOAA CLAMPS and SURFRAD, UW MRR and PIP 915 MHz wind profiler
Twitchell Island, CA <sub>9,13</sub>	US-Twt	D. Baldocchi and NOAA	CRO	boundary layer sounding	2017-	915 MHz wind profiler
Kansas Field Station, KS <sub>14</sub>	US-KFS	N. Brunsell	GRA	boundary layer height, cloud base and amount; backscatter profile	2016-	Vaisala CL51 lidar ceilometer
Graswang, Germany <sub>15</sub>	DE-Gwg	M. Mauder (TERENO)	GRA	boundary layer height, cloud base and amount; backscatter profile	2012-	Vaisala CL51 lidar ceilometer
Rottenbuch, Germany <sub>15</sub>	DE-RbW	M. Mauder (TERENO)	GRA	boundary layer height, cloud base and amount; backscatter profile	2012-	Vaisala CL51 lidar ceilometer
Fendt, Germany <sub>15</sub>	DE-Fen	M. Mauder (TERENO)	GRA	boundary layer height, cloud base and amount; backscatter profile	2012-	Vaisala CL51 lidar ceilometer
NY State Mesonet (17 sites, co-located atmos. and eddy covariance measurements) <sub>16</sub>	-	C. Thorncroft	various	atmospheric profiles: winds up to 7km above the surface; temperature and liquid up to 10km above the surface	2018-	Leosphere WindCube WLS-100 series Doppler LiDAR; Radiometrics MP-3000A Microwave Radiometer
Ruisdael Obs., Netherlands <sub>17</sub>	multiple	H. Russchenberg	various	various	in dev.	multiple instruments for in situ characterization of physical and chemical properties of the atmosphere
Selhausen Juelich ecosystem site <sub>18</sub>	DE-RuS	M. Schmidt	CRO	boundary layer height, cloud base and amount; backscatter profile, wind profiles, air temperature and humidity profiles	2007-	LufftCHM15k and Vaisala CT25k lidar ceilometer, HALO Doppler wind lidar, radiosondes, microwave radiometer
Renon <sub>19</sub>	IT-Ren	S. Minerbi	ENF	vertical profiles of wind velocity, backscatter profile	2000	Doppler Sodar Remtech PA1
Guadiana <sub>20</sub>	ES-Gdn	P. Serrano Ortiz	EBF	vertical and temporal evolution of atmospheric water vapor and aerosols, wind profiles, air temperature and humidity profiles	2016, 2019	HALO Doppler lidar, scanning Raman lidar, radiosondes
Tharandt <sub>21</sub>	DE-Tha	C. Bernhofer	ENF	vertical profiles of wind and turbulence, air temperature and humidity profiles	2016	tethered Vaisala balloon sonde, Metek Doppler-SODAR PCS2000-64/MF
Grillenburg <sub>22</sub>	DE-Gri	C. Bernhofer	GRA	line- and area-averaged wind components and acoustic virtual temperature [100 × 100 m <sup>2</sup> ], path-	2016	acoustic travel-time tomography, Bruker EM27 Open Path Spectrometer (OP-FTIR)

(continued on next page)

**Table 3 (continued)**

Location	Site Code	Contact	Ecosystem	Measurements	Period	Instrument(s)
Yatir Forest <sup>23</sup>	IL-YAT	D. Yakir	ENF	averaged concentrations of greenhouse gases [100 × 100 m <sup>2</sup> ] boundary layer height, cloud base and amount; backscatter profile	2015-	Vaisala CL51 ceilometer
Lannemezan <sup>24</sup>	-	S. Derrien	mixed	vertical wind profiles, air temperature and humidity profiles, boundary layer height, cloud base and amount; backscatter profile	2010-	Wind profiler radar, radiosondes, ceilometer
Hyltemossa <sup>25</sup>	SE-Htm	M. Heliasz	ENF	boundary layer height, cloud base and amount; backscatter profile	2017-	Vaisala CL51 ceilometer
Svartberget <sup>26</sup>	SE-Svb	P. Smith	ENF	boundary layer height, cloud base and amount; backscatter profile	2018-	Vaisala CL51 ceilometer
Norunda <sup>27</sup>	SE-Nor	M. Mölder	ENF	boundary layer height, cloud base and amount; backscatter profile	2018-	Vaisala CL51 ceilometer
Tapajos National Forest, Brazil	BR-SA1	S. Saleska and S. Wofsy	EBF	cloud base, backscatter profile	2001- 2003	Vaisala CT-25K ceilometer

<sup>1</sup><https://www.osti.gov/biblio/808114-regional-forest-abl-coupling-influence-co-sub-climate-progress-date>; <sup>2</sup>[https://daac.ornl.gov/cgi-bin/dsviewer.pl?ds\\_id=240](https://daac.ornl.gov/cgi-bin/dsviewer.pl?ds_id=240); <sup>3</sup><https://www.sciencedirect.com/science/article/pii/S0168192311000244>; <sup>4</sup><https://www.arm.gov/capabilities/observatories/sgp>; <sup>5</sup><https://www.arm.gov/capabilities/observatories/nsa>; <sup>6</sup><https://www.sciencedirect.com/science/article/pii/S0168192317300308>; <sup>7</sup><https://ameriflux.lbl.gov/sites/siteinfo/US-Wrc>; <sup>8</sup><https://ameriflux.lbl.gov/sites/siteinfo/US-Ho1>; <sup>9</sup><https://sites.psu.edu/influx/>; <sup>10</sup><https://ameriflux.lbl.gov/sites/siteinfo/US-Wkg>; <sup>11</sup><https://ameriflux.lbl.gov/sites/siteinfo/US-Whs>; <sup>12</sup>[https://www.eol.ucar.edu/field\\_projects/cheesehead](https://www.eol.ucar.edu/field_projects/cheesehead); <sup>13</sup>[https://www.esrl.noaa.gov/psd/data/obs/sites/view\\_site\\_details.php?siteID=tci](https://www.esrl.noaa.gov/psd/data/obs/sites/view_site_details.php?siteID=tci); <sup>14</sup><https://ameriflux.lbl.gov/sites/siteinfo/US-KFS>; <sup>15</sup><https://www.tereno.net>; <sup>16</sup><http://nysmesonet.org/about/welcome>; <sup>17</sup><http://ruisdael-observatory.nl/>; <sup>18</sup>[https://www.fz-juelich.de/ibg/ibg-3/EN/Research/Terrestrial\\_observationPlatforms/ICOS/Selhausen\\_agricultural\\_station/\\_node.html](https://www.fz-juelich.de/ibg/ibg-3/EN/Research/Terrestrial_observationPlatforms/ICOS/Selhausen_agricultural_station/_node.html); <sup>19</sup><https://deims.org/5d32cbf8-ab7c-4acb-b29f-600fecb30a1d>; <sup>20</sup><https://www.ugr.es/~andyk/pubs/066.pdf>; <sup>21</sup><http://www.icos-infrastruktur.de/en/icos-d/komponenten/oekosysteme/beobachtungsstandorte/tharandt-c1/>; <sup>22</sup><http://sites.fluxdata.org/DE-Gri/>; <sup>23</sup><https://www.weizmann.ac.il/EPS/Yakir/biosphere-atmosphere-fluxes>; <sup>24</sup><http://p2oa.aero.obs-mip.fr/spip.php?rubrique125&lang=fr>; <sup>25</sup><https://www.icos-sweden.se/hyltemossa>; <sup>26</sup><https://www.icos-sweden.se/svartberget>; <sup>27</sup><https://www.icos-sweden.se/norunda>; <sup>27</sup>[https://daac.ornl.gov/LBA/guides/CD03\\_Ceilometer\\_Km67.html](https://daac.ornl.gov/LBA/guides/CD03_Ceilometer_Km67.html)

**Table 4**

Summary of research directions that would substantially benefit from co-located eddy covariance surface flux and atmospheric boundary layer (ABL) observations. The most useful atmospheric variables and the recommended site setup are given for each research direction.

	Most useful variables				Site setup	
	Atmospheric boundary layer height	Air temperature and humidity profiles	Wind profiles	Cloud base height and cover	Single tower	Tower network or paired towers
<b>Interpretation of surface flux measurements</b>						
Understanding feedbacks between surface fluxes and atmosphere	x				x	
Linking atmospheric profiles and stability conditions to surface flux observations	x	x	x		x	
Interpreting spatial patterns of evaporation rates	x					x
Validating techniques to estimate regional evaporation rates	x	x			x	
Impacts of land cover and land surface heterogeneity on near-surface climates	x	x	x			x
Understanding turbulence transport in mountainous terrain	x			x		x
<b>Improving quality of eddy covariance flux measurements</b>						
Improving quality control of eddy covariance flux measurements				x		x
Interpreting nighttime eddy covariance flux measurements		x		x		x
Reducing uncertainties in flux footprint estimates	x					x
<b>Regional-scale modeling</b>						
Inferring regional-scale fluxes	x				x	
Bridging gap between inverse flux modeling and surface flux observations	x	x	x	x		x
<b>Land-atmosphere coupling and model validation</b>						
Validating land-atmosphere modeling efforts	x	x			x	x
Quantifying land-atmosphere coupling across biomes	x	x				x
Understanding vegetation-cloud interactions	x				x	x
Development of test-bed sites/networks	x	x	x	x	x	x
Validating spaceborne ABL missions	x	x	x			x

The growth of the ABL is directly coupled to land surface conditions and is influenced by feedback mechanisms between the surface energy balance and the entrainment of dry and warm air from above the ABL. Enhanced entrainment of drier free tropospheric air increases atmospheric water demand from vegetation and soils and can lead to an increase in surface latent heat flux and a concurrent reduction in surface

sensible heat flux. Under well-watered conditions (i.e., with sufficiently high soil moisture), surface latent heat flux continues to increase, which in turn moistens the ABL, lowers soil moisture (van Heerwaarden et al., 2009; Seneviratne et al., 2010; Santanello et al., 2018), and reduces ABL growth (e.g., McNaughton and Spriggs, 1986; van Heerwaarden et al., 2009; Salvucci and Gentile, 2013). However, stomata closing in

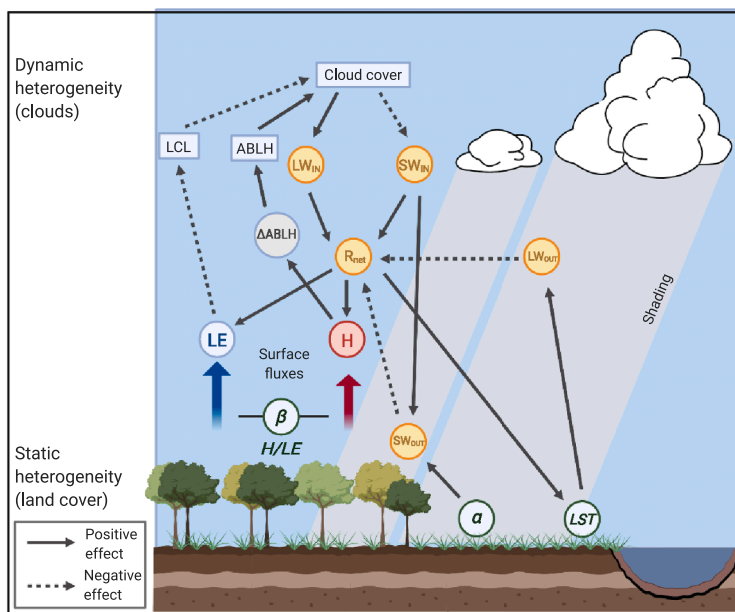


**Fig. 10.** Daytime feedbacks between cloud cover, radiative fluxes (net radiation [ $R_{net}$ ], incoming shortwave [ $SW_{IN}$ ] and longwave radiation [ $LW_{IN}$ ], outgoing shortwave [ $SW_{OUT}$ ] and longwave radiation [ $LW_{OUT}$ ]), surface energy fluxes (i.e., sensible heat flux [ $H$ ], latent heat flux [ $LE$ ]), land surface properties (albedo [ $\alpha$ ], land surface temperature [ $LST$ ], and Bowen ratio [ $\beta$ ]), and state of the atmospheric boundary layer (atmospheric boundary layer height [ $ABLH$ ] and its growth rate [ $\Delta ABLH$ ], and lifting condensation level [ $LCL$ ]). While cloud cover and patterns can change on short timescales (< 30 mins, dynamic heterogeneity), land cover patterns are relatively static on shorter timescales (< 1 month, static heterogeneity).

response to increasing vapor pressure deficit or to decreasing soil moisture reduces surface conductance and can reduce latent heat flux leading to a concurrent increase in sensible heat flux (i.e., increasing Bowen ratio; Helbig et al., 2020b; Lansu et al., 2020). In addition, cloud formation and precipitation occurrence are tightly coupled to ABL growth dynamics (Konings et al., 2010). If the ABLH reaches the LCL, condensation occurs, and convective clouds may form (Fig. 6). While the associated increase in diffuse radiation can positively affect photosynthetic uptake (Niyogi et al., 2004; Knoll and Baldocchi, 2008), cloud formation also reduces the amount of solar radiation that reaches the Earth's surface (Juang et al., 2007a; Vilà-Guerau de Arellano et al., 2014, see Fig. 10). This reduction in available energy at the land surface can exert a negative feedback on surface energy fluxes. For example, the impact of cloud cover on surface energy fluxes and ABL growth dynamics was seen during the CHEESEHEAD19 field campaign in Wisconsin (Butterworth et al., 2021) on two consecutive days with different degrees of cloud cover (Fig. 9). The cloudy day showed a delayed onset of ABL development and large reductions in sensible and latent heat fluxes, while the sunny day showed a more typical diurnal cycle with surface energy fluxes peaking midday and a rapidly growing ABL.

**Surface fluxes and atmospheric stability are strongly coupled via turbulent mixing and, thus, atmospheric profile measurements of temperature and specific humidity (needed to derive atmospheric stability) and wind may improve our understanding of the dynamic interaction between surface fluxes and atmospheric conditions.** For example, aerodynamic coupling between the land surface and the ABL affects the surface energy balance and is primarily controlled by atmospheric stability. During unstable conditions, a negative feedback occurs: an increase in surface temperature increases convective instability, turbulent mixing, and aerodynamic conductance, resulting in an increase in sensible heat flux. This increase in sensible heat flux acts to reduce surface temperature. During stable atmospheric conditions, temperature profiles are inverted, and turbulence is damped. Over well-watered surfaces (e.g., lakes, wetlands, or flooded/irrigated sites), the downward transport of sensible heat can feed evaporation and evaporative cooling of the surface reinforcing the temperature inversion and promoting further stable stratification (Brakke et al., 1978; Lang et al., 1974; Lang et al., 1983).

The ABLH represents the vertical extent of the atmosphere that is directly influenced by the Earth's surface (Fig. 1). Therefore, the ABLH

has been used as a scaling parameter under a range of atmospheric stability conditions (Zilitinkevich et al., 2012; Banerjee and Katul, 2013; Banerjee et al., 2015; Banerjee et al., 2016) to characterize the exchange between the land surface and the atmosphere. The measurement of ABLH alongside land-atmosphere exchange can therefore help constrain surface fluxes. On the other hand, the ABLH itself is a function of the sensible heat flux gradient across the ABL. Thus, over flat and homogeneous surfaces, the ABLH can be computed by a thermodynamic encroachment model:

$$\frac{dh}{dt} = \frac{\overline{w' \theta'} - \overline{w' \theta'_h}}{\gamma h} \quad (1)$$

where  $h$  is the ABLH,  $\overline{w'\theta'}$  is the kinematic sensible heat flux at the surface,  $\overline{w'\theta_h'}$  is the entrainment flux at the ABL top, and  $\gamma$  denotes the potential temperature gradient of the free atmosphere above the ABL (e.g., Tennekes, 1973; Zilitinkevich et al., 2012; Brugger et al., 2018). The entrainment heat flux is often modeled as a fixed proportion of the surface heat flux. Equation 1 approximates the ABL as a single slab without any internal source and sink terms. Integrating equation 1 (Brugger et al., 2018) or more complex ABL growth formulations (e.g., Driedonks and Tennekes, 1984) offers a technique to couple eddy covariance flux measurements and ABLH observations at a particular site (Batchvarova and Gryning, 1991; Brugger et al., 2018).

Additionally, profiles of wind and air temperature in the lowest levels of the ABL (i.e., the roughness sublayer, the surface layer, and into the lower mixed layer, see Fig. 3) can provide critical information for extrapolating the influence of vegetation structure and function at the surface into the ABL. The parameters of the Monin-Obukhov Similarity Theory functions for the diabatic profiles of wind and temperature (Monin and Obukhov, 1954) depend on measured fluxes (e.g., momentum and sensible heat), as well as scaling parameters like the zero-plane displacement and roughness lengths for momentum and heat (which themselves are strongly affected by canopy structure, Brutsaert 1982). Properly constraining the parameters of these profile equations is made substantially easier if at least one, and ideally multiple, observations of the key scalars (air temperature, wind speed) are made within the surface layer, which is often assumed to extend from a height of 2-5 times the height of the canopy (i.e., local blending height) to about 10% of the ABL height (Raupach and Thom, 1981). For ecosystems with short

canopy heights (i.e., grasslands, croplands), many existing flux tower heights extend into the surface layer (Fig. 3), substantially facilitating the application of similarity theory. However, for forests and woodlands, most flux tower heights are constrained to within the roughness sub-layer, where diabatic profile functions do not apply due to local, near-surface canopy drag effects (Harman and Finnigan, 2007; Harman and Finnigan, 2008). At these sites, additional information about the profiles of temperature and wind in the surface layer (for example, from radiosonde observations or sodar) could better constrain estimates of the zero-plane displacement and roughness lengths, and better facilitate the transfer of information about measured fluxes to their impacts on atmospheric state variables throughout the ABL (e.g., Novick and Katul, 2020).

**ABL growth observations can help interpret differences in measured evaporation rates over a spectrum of sites from well-watered and productive to dry, sparse and unproductive.** Evaporation of an extended wet surface exceeds the equilibrium rate of evaporation ( $LE_{eq}$ ) through the coupling mechanisms between land surface and ABL. This effect can be best demonstrated by applying a coupled ABL model (McNaughton and Spriggs, 1986) that links the Penman-Monteith equation to a simple one-dimensional slab ABL model. Evaporation rates depend on the vapor pressure deficit within the ABL, whose growth and entrainment depend on sensible heat flux at the surface (e.g., Raupach, 2000; Raupach, 2001). Under conditions of low surface resistance (i.e., well-watered conditions), the ratio of actual evaporation to  $LE_{eq}$  approaches 1.26 because of this coupling (i.e., Priestley-Taylor coefficient; Priestley and Taylor, 1972). If well-watered surfaces are isolated within a drier landscape (e.g., irrigated land), large regional sensible heat flux and enhanced vapor pressure deficit can accelerate water losses to the atmosphere and lead to ratios of actual evaporation to  $LE_{eq}$  well above 1.26 (Shuttleworth et al., 2009; Baldocchi et al., 2016). In such cases, direct measurements of ABLH and of temperature and humidity profiles are crucial to interpret the large observed evaporation rates.

**Observations of atmospheric temperature and humidity profiles and ABL growth across flux tower sites can provide unique datasets to validate techniques to estimate regional evaporation rates** (e.g., Rrigden and Salvucci, 2015). One of the outstanding challenges to computing land atmosphere fluxes is assessing the down regulation of stomatal (and surface) conductance as soil moisture deficits increase (Fig. 4). The lack of consistent and large-scale soil moisture observations poses another challenge to this task. Recent work, demonstrating how plants can act as a “sensor” for soil moisture, has highlighted their influence on the humidification of the ABL (e.g., Pedruzo-Bagazgoitia et al., 2017; Vilà-Guerau de Arellano et al., 2014; Combe et al., 2016; Denissen et al., 2021). The vertical variance of the relative humidity profile within the ABL can be used to infer the large-scale surface conductance from weather station data only (Gentine et al., 2016; Salvucci and Gentine, 2013). Due to the tight coupling of latent heat exchange at the land surface and atmospheric humidity and temperature, this approach can serve as an inferential measure of land surface conditions (e.g., soil moisture) at large spatial scales (McColl and Rigden, 2020) and has been shown to produce estimates of evapotranspiration rates across North America comparable to a range of other evapotranspiration data products (Rrigden and Salvucci, 2015). Co-located continuous measurements of ABLH, temperature and humidity profiles, and surface fluxes can provide an important tool to test the validity of these new approaches.

**Analyses of land use and cover impacts on near-surface climates can be expanded across the FLUXNET network but require both direct ABL measurements and models to interpret observations.** Recent work has assessed how land use and cover affects local air temperatures through land surface-atmosphere interactions (Lee et al., 2011; Baldocchi and Ma, 2013; Helbig et al., 2016; Hemes et al., 2018; Helbig et al., 2020a; Novick and Katul, 2020). To quantify such effects on local near-surface and regional climate, the coupling between land surface, ABL, and free troposphere needs to be accounted for (van Heerwaarden

et al., 2009). Similarly, co-location of flux towers and ABL observations in urban environments can help better understand the effect of urban planning on near-surface climate and air pollution and thus on human health and comfort (e.g., Kotthaus and Grimmond, 2018b; Wood et al., 2013).

Apart from surface heating and cooling, the ABL height is also highly sensitive to land surface cover, topography, and synoptic conditions. While a number of studies have investigated the changes in ABLH with atmospheric stratification, studies on the impact of surface heterogeneity and land-cover transitions on ABLH are scarce. Brugger et al. (2018) investigated the influence of surface heterogeneity on ABLH in the context of a semi-arid forest surrounded by a shrubland (i.e., Yatir forest in the Negev desert, Israel). The presence of a large-scale surface heterogeneity violated the assumption of planar homogeneous conditions; however, an internal boundary layer model originally conceptualized by Venkatram (1977) and modified by Brugger et al. (2018) was used to compute the change of ABLH due to the surface roughness transition. This spatially explicit model accounts for turbulent fluxes measured by eddy covariance towers over the different surfaces and the geometric configuration of the transition and couples these measurements with the mixed layer and ABL measurements over the land surfaces. For example, a transition from a shrubland to forest results in the growth of an internal boundary layer, which assumes a vertical transport of the forest's effects at the convective velocity scale to the ABL top while being advected horizontally at the same time by the background flow. (Kröniger et al., 2018) conducted large eddy simulation over the same site and was able to validate this model and the eddy covariance measurements along with ABL models were useful to interpret the results, especially to investigate the role of secondary circulations that could further modulate land-atmosphere exchange (Banerjee et al., 2018). Similar modeling exercises reinforced with co-located eddy covariance surface flux and ABL measurements could be beneficial for other applications such as models for regional climate, pollutant transport, and urban heat islands.

**Combining surface flux and continuous ABL observations can be an effective approach to disentangle complex transport mechanisms in mountainous terrain and to resolve the non-prototypical multi-layered structure of mountainous boundary layers.** Eddy covariance flux measurements in complex mountainous terrain have been successfully conducted despite the typical diurnal development of regional wind systems (e.g., Hammerle et al., 2007; Hiller et al., 2008). Surface energy flux observations from flux towers can contribute to a better understanding of turbulence over complex terrain and thus of ABL development in mountainous terrain, which results from diverse transport processes (e.g., orographic gravity waves, thermally driven circulation; see Kutter et al., 2017 and Serafin et al., 2018). The complexity of mountainous ABL development is also reflected in the mismatch between CBL heights and mixing heights (i.e., aerosol layer). Aerosol layer heights can be substantially higher due to mountain venting processes caused by slope flows in mountainous terrain (e.g., De Wekker et al., 2004). For a more detailed discussion of mountainous boundary layers, the reader is directed to the work by Lehner and Rotach (2018) and Serafin et al. (2018).

## 5.2. Improving quality of eddy covariance flux measurements

**Atmospheric boundary layer observations can provide important information on the state of the atmosphere and can thus improve quality control of eddy covariance fluxes.** The quality of eddy covariance flux measurements varies with atmospheric conditions and depends on the fulfilment of fundamental micrometeorological assumptions (e.g., negligible advective fluxes). The influence of regional or mesoscale (i.e., non-local) motions on turbulent exchange between the land and atmosphere have often been studied using short-term, campaign-style observations (e.g., Shen and Leclerc, 1995, Aubinet et al., 2010). Such studies revealed the effect of certain ABL processes on

uncertainties in eddy covariance flux measurements emphasizing the need for continuous ABL measurements at flux tower sites. These observations could for example detect large vertical exchanges of air within the canopy, which can originate from the ABL and be important particularly in tall (e.g., forest) canopies (e.g., Thomas and Foken, 2007; Wharton et al., 2017). Non-local motions can occur at larger timescales than those typically associated with canopy transport and eddy covariance averaging intervals. (Patton et al., 2016) argue that single point (e.g., tower) observations should be averaged over time scales of the ABL motions rather than of canopy-scale transport processes. There is evidence that inability to resolve large eddies that entrain warm-dry air in traditional eddy covariance flux calculation methodology may contribute to the lack of surface energy balance closure, which leads to systematic underestimation of energy and possibly of carbon fluxes at most flux tower sites (Stoy et al., 2013; Eder et al., 2015b; Mauder et al., 2020). Continuous ABL observations of wind speed and direction could be used to identify periods when these eddies are present and be used to correct or flag biased flux measurements (de Roo et al., 2018).

**Interpretation of nighttime fluxes is a major focus for the integration of ABL and eddy covariance flux measurements.** Friction velocity ( $u^*$ ) thresholds are commonly applied as a proxy for inadequate turbulent mixing whereby periods below the  $u^*$  thresholds are removed from the estimate of the nighttime CO<sub>2</sub> (respiration) flux and subsequently gap-filled. While the appropriateness of  $u^*$  thresholds remain highly debated (Acevedo et al., 2009), others have focused on understanding the mechanisms for when nocturnal turbulence can be enhanced, particularly by non-local flows (e.g., low-level jets, Karipot et al., 2006; El-Madany et al., 2014; Wharton et al., 2017). Wharton et al. (2017) used wind-profiling lidar to identify two different non-local motions (downslope flow and intermittent turbulence) and applied different turbulent parameters for estimating canopy mixing during those periods at two flux tower sites. They found that nocturnal canopy turbulence was the result of a complex interaction of non-local flows and atmospheric stability, which could not be assessed solely by  $u^*$ . For the case of nocturnal low-level jets, Prabha et al. (2008) invoked a shear-sheltering hypothesis, requiring vertical wind profiles, to identify cases when the low-level jet enhanced turbulent mixing. Without more (and continuous) ABL observations at eddy covariance flux towers, nighttime fluxes may become biased through over-filtering (e.g., application of  $u^*$  thresholds). However, relying on overstory  $u^*$  can also lead to overestimation of periods of adequate turbulence mixing in the canopy at some sites. For example, at the Tonzi AmeriFlux site, nighttime katabatic flows produced shear at heights near the top of the flux tower (Wharton et al., 2017) resulting in elevated turbulence seen in the relatively high overstory  $u^*$  values. At the same time,  $u^*$  at the bottom of the “open” canopy was low and indicating low canopy mixing. In this case, a finer resolution temperature and wind profile is needed to adequately quantify canopy mixing strength.

**Continuous measurements of ABLH dynamics co-located with eddy covariance flux measurements could reduce uncertainties in current flux footprint estimates and thereby help identifying source and sink hotspots.** Flux footprint models provide an important tool to determine the location and extent of the source area of impact to eddy covariance flux measurements, to identify greenhouse gas sources and sinks within the source area, and to improve interpretation of the measured fluxes (Vesala et al., 2008; Barcza et al., 2009; Griebel et al., 2016; Xu et al., 2017). Footprint estimates either directly (via input parameter) or indirectly (via mixing volume) depend on the ABLH (Kljun et al., 2015). This dependence is critical especially for the case of stable atmospheric conditions due to a shallow ABL that can act as a “lid” for sources-sinks, and because nighttime stable footprints typically extend much longer than the typical convective daytime footprints, thus opening opportunities to interpret greenhouse gas and energy fluxes originating from more distant sources (Kljun et al., 2002; Baldocchi et al., 2012). In the absence of direct measurements, ABLH is usually estimated using various modeling approaches (see Yi et al., 2001; Kljun et al., 2015). The

ABLH is also essential for footprint modeling when measurement height is greater than 10% of ABLH, which occurs during early mornings or with very tall towers (Kljun et al., 2015; Wang et al., 2006).

### 5.3. Regional scale modeling

**Atmospheric boundary layer height measurements can be used with additional concentration measurements to infer budgets of conserved scalars such as CO<sub>2</sub> or methane beyond the flux tower footprint scale** (Wofsy et al., 1988; Styles et al., 2002; Bakwin et al., 2004; Betts et al., 2004; Helliker et al., 2004; Yi et al., 2004; Wang et al., 2007; Pino et al., 2012). Raupach et al. (1992) describe the CBL budget approach that assumes the bulk of the ABL is well mixed, the surface layer (affected by surface fluxes) is thin, and that the ABLH growth is rapid in comparison to subsidence from the atmosphere above (see also Betts, 1992). These conditions may occur during the middle of sunny clear days when high pressure systems are dominant. Under these circumstances,

$$\frac{dC_m}{dt} = \frac{F_c}{h} + \left( \frac{C_+ - C_m}{h} \right) \frac{dh}{dt} \quad (2)$$

Where  $C_m$  is the average concentration of the scalar  $C$  throughout the well-mixed CBL,  $h$  is the CBL height,  $C_+$  is the concentration of the scalar in the free atmosphere just above the CBL, and  $F_c$  is the surface flux of the scalar. For example, Denmead et al. (1996) used this equation 2 in both differential and integral form to estimate regional water vapor and CO<sub>2</sub> flux over agricultural land. Furthermore, the convective budgeting approach was used in other regional budget studies such as FIFE (Betts and Ball, 1994), BOREAS (Barr and Betts, 1997), and at tall tower sites (Desai et al., 2010; Helliker et al., 2004). Cleugh and Grimmond (2001) tested and refined this approach over a mixed (rural to urban) landscape, while Baldocchi et al. (2012) used atmospheric budgeting to better understand anomalies in methane fluxes. However, this approach fails if advection contributes to changes in scalar concentrations. For example, the passage of frontal systems is accompanied by substantial changes in CO<sub>2</sub> concentrations in the ABL (Pal et al., 2020).

Denmead et al. (1996) also discussed the potentially simpler issue of NBL budgeting. During nights with strong temperature inversions, the ABL collapses to heights of only tens of meters, trapping surface emissions in a shallow layer. Monitoring the time rate of change of a scalar ( $C$ ) through the inversion to height  $h$  yields a flux ( $F_c$ ),

$$F_c = \int_0^h \frac{dC}{dt} dh \quad (3)$$

Note that it is during strongly stable, nocturnal periods characterized by an absence of turbulence, when the eddy covariance method fails. The NBL budget method (equation 3) was first used with tethered balloons carrying sampling tubes leading to a ground-based analyzer (e.g., Choularton et al., 1995). The rapid advance of small unmanned aerial vehicles and their use in carrying CO<sub>2</sub> and other equipment for atmospheric measurement (e.g., Brady et al., 2016) suggest many new opportunities for the NBL budget method.

**Continuous ABL measurements would help to bridge the gap between flux towers and atmospheric inverse flux estimates.** In contrast to the CBL budget approach, atmospheric inverse analyses (e.g. Ciais et al., 2010) integrate atmospheric greenhouse gas concentration measurements from tower networks (Andrews et al., 2014; Miles et al., 2012), satellites (Kuze et al., 2016; Crisp et al., 2017) and aircraft (Sweeney et al., 2015) with atmospheric transport models to estimate regional (Lauvaux et al., 2012; Lauvaux et al., 2016; Barkley et al., 2019; Hartery et al., 2018) to global (Crowell et al., 2019; Peylin et al., 2013) surface fluxes. These methods simulate atmospheric advection, ABL winds, and ABL mixing, and in most cases should supersede the simple ABL budget methods (see above). Inverse analyses, however, are often limited in their temporal and spatial resolution, and in their regional

accuracy and precision, and are sensitive to transport model errors including ABL winds and ABLH (Basu et al., 2018; Lauvaux and Davis, 2014; McGrath-Spangler et al., 2015; Díaz-Isaac et al., 2018; Feng et al., 2019; Feng et al., 2020). ABL measurements at FLUXNET tower sites can enhance atmospheric inversion techniques in at least two ways.

First, atmospheric inverse flux estimates can in principle be compared to tower flux estimates. The different spatial and temporal resolutions of these methods make this challenging. Remote sensing, ecosystem models, and biomass data can be used to upscale flux measurements to bridge this gap (Davis, 2008; Xiao et al., 2014a; 2014b; Hilton et al., 2014; Jung et al., 2011). Flux towers are now being used to calibrate ecosystem model ensembles (Zhou et al., 2020), which can serve as probabilistic prior flux estimates for atmospheric inversion systems (Wesloh et al., 2020). Higher-resolution atmospheric inverse analyses (Lauvaux et al., 2012; Hu et al., 2019) also provide more opportunities for cross-evaluation of our understanding of the carbon cycle with the flux tower network.

Second, a network of co-located, continuous measurements of ABLH, mean wind profiles, and atmospheric turbulence profiles, all of which can be obtained with stationary profiling instruments such as Doppler lidars (Tucker et al., 2009), could be used to evaluate, improve, and calibrate these atmospheric inversion systems. Assimilation of Doppler lidar wind measurements has been demonstrated to improve atmospheric inverse flux estimates for an urban landscape (Deng et al., 2017). For example, ABLH and wind profiles from radiosondes have been used to evaluate (Díaz-Isaac et al., 2018) and calibrate (Díaz-Isaac et al., 2019; Feng et al., 2020) the mesoscale models that are used for regional flux inversion systems, but radiosonde observations have limited temporal resolution, and do not measure atmospheric turbulence, a key element of ABL mixing. Additionally, the numerical weather models used in atmospheric inversion systems are highly sensitive to land surface energy fluxes (Díaz-Isaac et al., 2018). Surface flux observation sites are thus an obvious choice for joint evaluation and improvement of ABL parameterizations in these numerical weather models and of the underlying land surface models.

#### 5.4. Land-atmosphere coupling and model validation

**Combining continuous and distributed observations of ABLH with turbulent fluxes would help to better validate local- to continental-scale land-atmosphere modeling efforts.** Models of various complexity and scales (including slab, single-column, large-eddy simulation (LES), regional, and Earth system models) have been used to increase our understanding of land-atmosphere coupling and feedback. While ABL observations at individual flux tower sites can be used to validate single-column models, distributed networks of ABL observations are needed to validate spatially explicit atmospheric models (such as mesoscale models used for atmospheric flux inversion techniques or coupled Earth system models). Validation of both types of models will increase capabilities to better understand the role of land cover, use, and management in ABL dynamics (e.g., Luyssaert et al., 2014; Helbig et al., 2016; Vick et al., 2016; Chen et al., 2017).

Slab-type column models, which only require estimates of the diurnal cycle of sensible and latent heat fluxes as well as atmospheric temperature and moisture lapse rates, have been commonly used to understand timing and onset conditions of ABL clouds or local convective precipitation (e.g., Juang et al., 2007a; Juang et al., 2007b; Gentile et al., 2013a; Gentile et al., 2013b; Manoli et al., 2016; Gerken et al., 2018a; Gerken et al., 2018b), to quantify the impact of land cover change on near-surface climates (e.g., Baldocchi and Ma, 2013; Luyssaert et al., 2014; Helbig et al., 2016; Helbig et al., 2020a), and have also been extended to include carbon and other atmospheric trace gas processes (e.g., Vilà-Guerau de Arellano et al., 2015). In the absence of direct ABL observations, numerical models, diagnostic equations, and empirical ABLH estimates can be useful for practical applications (e.g., Yi et al., 2001; Zilitinkevich and Baklanov, 2002) and can provide

insights into land-atmosphere interactions (e.g., van Heerwaarden and Teuling, 2013). However, CBL models and diagnostic equations for SBL are not universally applicable (e.g., Vickers and Mahrt, 2004), often require calibration of parameters, may introduce biases to ABLH estimates (e.g., Denning et al., 2008; Hu et al., 2010; Banks et al., 2015), and some ABL models require atmospheric profile measurements for initialization (Seibert et al., 2000). Direct ABL observations at flux tower sites are crucial to design and constrain numerical experiments for large-eddy simulations that can be used to improve or propose new parameterizations for existing CBL/SBL models and to validate the performance of surface exchange and turbulence parameterizations in weather, air quality, and climate models across a range of land cover types (Edwards et al., 2020). Single-site surface flux, ABLH, and atmospheric profiling measurements in relatively homogeneous regions would therefore provide a powerful tool for validating and improving ABL models and for evaluating local-scale land-atmosphere coupling.

Heterogeneous landscapes, and regional to continental scale simulations, however, require explicit consideration of the four-dimensional nature of the atmosphere and its interaction with the Earth's surface. Observations of surface fluxes and ABLH and winds have played an integral role in studies of mesoscale flows, in improving our understanding of ABL development over heterogeneous surfaces, and in the evaluation of numerical weather models. Many of the studies of mesoscale flows have relied upon airborne flux and ABL observations (e.g., Sun et al., 1997; Kang et al., 2007), or airborne ABL observations paired with regional flux tower networks (Desai et al., 2005; Reen et al., 2006; Reen et al., 2014). Evaluations of numerical weather models have not typically made extensive use of flux tower networks. The inclusion of ABL profiling measurements at FLUXNET sites would provide invaluable long-term grounding points for studies of mesoscale to continental-scale land-atmosphere interactions. No comparable data source currently exists.

**The combination of ground-based observations of surface fluxes and of ABLH allow for closure of ABL energy, water, and gas budgets and can help to quantify land-atmosphere coupling across biomes.** Land-atmosphere coupling mediates important feedback processes in weather and climate (e.g., Santanello et al., 2018). For example, lower soil moisture during compound drought and heatwaves is associated with higher sensible and lower latent heat fluxes and thus enhanced ABL growth and further warming (e.g., Sanchez-Mejia and Papuga, 2014; Sanchez-Mejia and Papuga, 2017). Such feedbacks - highly variable in space and time - are difficult to observe without extensive, continuous ABL and surface flux observations (Gerken et al., 2019; Koster et al., 2009) thus limiting our understanding of atmospheric processes (e.g., Betts, 2009; Ek and Holtslag, 2004; Santanello et al., 2018).

To facilitate validation of land-atmosphere coupling in models, the local land-atmosphere coupling (LoCo; Santanello et al. 2018) initiative under the GEWEX project has developed quantitative metrics to better understand land-atmosphere coupling in models and observations over the last decade. A key limitation to the application of these metrics is the lack of consistent and continuous (in time or space) measurements of ABL thermodynamics and ABLH. The 'process chain' connecting soil moisture-surface fluxes-ABL evolution-entrainment-clouds-precipitation relies on consistent, co-located observations of these variables, and to date most soil moisture or surface flux networks lack the corresponding ABL observations that are necessary to validate numerical weather models.

**The short and long-term responses of vegetation to the dynamics of boundary layer cloud development are still an open issue.** Tackling this land-atmosphere interaction with continuous, long-term ABL observations could help to reduce uncertainties related to the coupling of terrestrial uptake of CO<sub>2</sub> and ABL clouds, including their transitions. At sub-diurnal and sub-kilometer scales, it is necessary to further quantify how vegetation controls the partitioning between sensible and latent heat flux (Vilà-Guerau de Arellano et al.,

2012) and the impact on the cloud cycle (Sikma and Vilà-Guerau de Arellano, 2019). Flux tower clusters with multiple surface flux and ABL observation systems are uniquely poised to provide important information on the effect of spatio-temporal variability of surface fluxes, cloud cover, and ABLHs on regional land-atmosphere interactions (e.g., Beyrich et al., 2006; Xu et al., 2020). These observational studies will require dedicated observations of ABL growth dynamics, of stable isotopologues (Griffis et al., 2007), of the partitioning of direct and diffuse radiation (Pedruzo-Bagazgoitia et al., 2017), and of leaf-level stomatal conductance (Vilà-Guerau de Arellano et al., 2020) to identify complex coupling between photosynthesis, evapotranspiration, and cloud cover dynamics.

**Flux tower sites with continuous ABL observations could expand on the idea of test-bed sites** such as the U.S. Department of Energy (DOE) Atmospheric Radiation Measurement (ARM) user facility sites with the LASSO (Large-Eddy Simulation ARM Symbiotic Simulation and Observation) project (Gustafson et al., 2020) or the Royal Netherlands Meteorological Institute Parameterization Testbed (Netherlands et al., 2012) that integrate observations with LES, slab models, and operational weather forecasting models. In this context, ABL observations could be used to diagnose entrainment fluxes of water, energy, and atmospheric trace gases at the ABL top (Santanello et al., 2009; Santanello et al., 2011) or to elucidate the surface and atmospheric controls on convective precipitation over wet and dry soils (e.g., Findell and Eltahir, 2003a; Findell and Eltahir, 2003b; Ford et al., 2015; Yin et al., 2015). Recently, the role of land-atmosphere feedbacks in expansion and intensification of droughts and heatwaves has been highlighted (Miralles et al., 2014; 2019). Given the importance of droughts and heatwaves for the carbon cycle (Wolf et al., 2016), water resource and wildfire management, agriculture, and human health, the combined surface flux and ABLH observations across the FLUXNET network have the potential to contribute to better quantification of these feedback processes, arising from cumulative drying of soils, increased surface flux partitioning toward sensible heat flux, and subsequent heat accumulation in the ABL (Miralles et al., 2014).

**Future spaceborne missions have the potential to provide improved spatial coverage of ABL observations and to connect local (i.e., flux tower) to regional scales, but require ground-based observations for validation.** An improved spatial and temporal coverage of ABL observations at flux tower sites would enable enhanced calibration and validation efforts, process understanding, and retrieval constraints for such spaceborne ABL missions. The 2017 ESAS Decadal Survey (National Academies of Sciences, Engineering, and Medicine 2018) has recommended ABL thermodynamic profiles and ABLH as most critical measurements from space for a range of scientific applications, such as those discussed above. NASA is devoting the next decade to ‘incubate’ new approaches and technologies that can lead to future ABL missions and provide globally continuous measurements of ABL properties. This incubation will rely heavily on knowledge and technology developments demonstrated by ground-based networks. The improved coverage and co-location of ground-based ABL observations at FLUXNET sites would provide crucial information for developing a strategy for ABL observations from space, in addition to ongoing ground-validation of remote measurements.

## 6. Conclusions

Atmospheric boundary layer measurements provide important observations to address pressing research questions. Many land-atmosphere studies at eddy covariance flux tower sites have relied on modeling approaches due to the lack of direct ABL observations (e.g., Baldocchi and Ma, 2013; Helbig et al., 2016; Lansu et al., 2020) or have made use of radiosonde observations that are restricted by limited temporal resolution or by proximity to the site (e.g., Juang et al., 2007b). New measurement technologies have become available recently enabling continuous, high-frequency ABL observations across the

FLUXNET network, opening new perspectives on the complex feedbacks between the land surface and the atmosphere.

Our review demonstrates that efforts to expand the availability of ABL observations across the FLUXNET network, either through new instrument deployments or campaigns to make previously collected data available, would allow the Earth science community to address new emerging research questions. Joint ABL and surface flux observations would also increase the usability of flux tower observations by the broader research communities (e.g., remote sensing, Earth system modelling, atmospheric science). Adding ABL measurements to more sites within the FLUXNET network, spanning a range of ecosystem types, climate zones and terrain, and systematic efforts to make new and existing ABL measurements available from network platforms, would

- (1) lead to better understanding of complex feedbacks between surface flux and ABL dynamics,
- (2) support flux footprint modelling, the interpretation of surface fluxes in heterogeneous and mountainous terrain, and quality control of eddy covariance flux measurements
- (3) support efforts to upscale surface fluxes from local to regional scales, and
- (4) provide essential data for the validation of land-atmosphere coupling in Earth system models and of spaceborne ABL missions,

There is an urgent need to develop the observational infrastructure, to share best practices among flux tower site teams, and to develop protocols and standardized data formats to enable efficient sharing of ABL data (i.e., ABLH, air temperature, humidity, wind, and flux profiles, cloud cover and cloud base height). Combining ABL observations with eddy covariance-based surface flux measurements would produce unique observational datasets for studies of land-atmosphere interactions and would thus add substantial value to ongoing flux tower measurements.

## Declaration of Competing Interest

The authors declare that they have no known competing financial interests or personal relationships that could have appeared to influence the work reported in this paper.

## Acknowledgments

ADR acknowledges support from the Department of Energy (DE-SC0017167) and National Science Foundation (DEB-1702697). Lawrence Livermore National Laboratory is operated by Lawrence Livermore National Security, LLC, for the U.S. Department of Energy, National Nuclear Security Administration under Contract DE-AC52-07NA27344. ARD acknowledges support from the DOE Ameriflux Network Management Project and NSF #1822420. Observations from the Atmospheric Radiation Measurement (ARM) user facility are supported by the U.S. Department of Energy (DOE) Office of Science user facility managed by the Biological and Environmental Research Program. Work at ANL was supported by the U.S. Department of Energy, Office of Science, Office of Biological and Environmental Research, under contract DE-AC02-06CH11357. KJD and TG acknowledge support from NASA’s Earth Science Division via Grant NNX15AG76G. KJD also acknowledges support from NIST via grant 70NANB19H128. Figs. 1, 3, 4, 8, and 10 were created with Biorender.com.

## Supplementary materials

Supplementary material associated with this article can be found, in the online version, at doi:10.1016/j.agrformet.2021.108509.

## References

- Acevedo, O.C., Moraes, O.L.L., Degrazia, G.A., Fitzjarrald, D.R., Manzi, A.O., Campos, J.G., 2009. Is friction velocity the most appropriate scale for correcting nocturnal carbon dioxide fluxes? *Agric. For. Meteorol.* 149 (1), 1–10.
- Andrews, A.E., Kofler, J.D., Trudeau, M.E., Williams, J.C., Neff, D.H., Masarie, K.A., Chao, D.Y., Kitzis, D.R., Novelli, P.C., Zhao, C.L., Dlugokencky, E.J., Lang, P.M., Crotwell, M.J., Fischer, M.L., Parker, M.J., Lee, J.T., Baumann, D.D., Desai, A.R., Stanier, C.O., De Wekker, S.F.J., Wolfe, D.E., Munger, J.W., Tans, P.P., 2014. CO<sub>2</sub>, CO, and CH<sub>4</sub> measurements from tall towers in the NOAA earth system research laboratory's global greenhouse gas reference network: instrumentation, uncertainty analysis, and recommendations for future high-accuracy greenhouse gas monitoring efforts. *Atmos. Meas. Tech.* 7 (2), 647–687.
- Angevine, W.M., Edwards, J.M., Lothon, M., LeMone, M.A., Osborne, S.R., 2020. Transition periods in the diurnally-varying atmospheric boundary layer over land. *Boundary Layer Meteorol.* 177, 205–223.
- Angevine, W.M., White, A.B., Avery, S.K., 1994. Boundary-layer depth and entrainment zone characterization with a boundary-layer profiler. *Boundary Layer Meteorol.* 68 (4), 375–385.
- Aubinet, M., Feigenwinter, C., Heinesch, B., Bernhofer, C., Canepa, E., Lindroth, A., Montagnani, L., Rebmann, C., Sedlak, P., Van Gorsel, E., 2010. Direct advection measurements do not help to solve the night-time CO<sub>2</sub> closure problem: evidence from three different forests. *Agric. For. Meteorol.* 150 (5), 655–664.
- Bakwin, P.S., Davis, K.J., Yi, C., Wofsy, S.C., Munger, J.W., Haszpra, L., Barcza, Z., 2004. Regional carbon dioxide fluxes from mixing ratio data. *Tellus* 56B, 301–311.
- Baldocchi, D.D., 2020. How eddy covariance flux measurements have contributed to our understanding of Global Change Biology. *Global Change Biol.* 26 (1), 242–260.
- Baldocchi, D.D., Hincks, B.B., Meyers, T.P., 1988. Measuring biosphere-atmosphere exchanges of biologically related gases with micrometeorological methods. *Ecology* 69 (5), 1331–1340.
- Baldocchi, D.D., Dettlof, M., Sonnentag, O., Verfaillie, J., Teh, Y.A., Silver, W., Kelly, N.M., 2012. The challenges of measuring methane fluxes and concentrations over a peatland pasture. *Agric. For. Meteorol.* 153, 177–187.
- Baldocchi, D.D., Knox, S., Dronova, I., Verfaillie, J., Oikawa, P., Sturtevant, C., Matthes, J.H., Dettlof, M., 2016. The impact of expanding flooded land area on the annual evaporation of rice. *Agric. For. Meteorol.* 223, 181–193.
- Baldocchi, D.D., Ma, S., 2013. How will land use affect air temperature in the surface boundary layer? Lessons learned from a comparative study on the energy balance of an oak savanna and annual grassland in California, USA. *Tellus B* 65 (1), 1994.
- Banerjee, T., Katul, G.G., 2013. Logarithmic scaling in the longitudinal velocity variance explained by a spectral budget. *Phys. Fluids* 25 (12), 125106.
- Banerjee, T., Katul, G.G., Salesky, S.T., Chamecki, M., 2015. Revisiting the formulations for the longitudinal velocity variance in the unstable atmospheric surface layer. *Q. J. R. Meteorol. Soc.* 141 (690), 1699–1711.
- Banerjee, Tirtha, Brugger, P., Roo, F.D., Kröninger, K., Yakir, D., Rotenberg, E., Mauder, M., 2018. Turbulent transport of energy across a forest and a semiarid shrubland. *Atmos. Chem. Phys.* 18 (13), 10025–10038.
- Banerjee, Tirtha, Li, D., Jiang, J.-Y., Katul, G., 2016. A spectral budget model for the longitudinal turbulent velocity in the stable atmospheric surface layer. *J. Atmospheric Sci.* 73 (1), 145–166.
- Banks, R.F., Tiana-Alsina, J., Rocadenbosch, F., Baldasano, J.M., 2015. Performance evaluation of the boundary-layer height from Lidar and the Weather Research and Forecasting model at an urban coastal site in the North-East Iberian Peninsula. *Boundary Layer Meteorol.* 157, 265–292.
- Banta, R.M., Mahrt, L., Vickers, D., Sun, J., Balsley, B.B., Pichugina, Y., Williams, E.J., 2007. The very stable boundary layer on nights with weak low-level jets. *J. Atmospheric Sci.* 64, 3068–3090.
- Barcza, Z., Kern, A., Haszpra, L., Kljun, N., 2009. Spatial representativeness of tall tower eddy covariance measurements using remote sensing and footprint analysis. *Agric. For. Meteorol.* 149 (5), 795–807.
- Barkley, Z.R., Davis, K.J., Feng, S., Balashov, N., Fried, A., DiGangi, J., Choi, Y., Halliday, H.S., 2019. Forward modeling and optimization of methane emissions in the South Central United States using aircraft transects across frontal boundaries. *Geophys. Res. Lett.* 46, 564–573.
- Barr, A.G., Betts, A.K., 1997. Radiosonde boundary layer budgets above a boreal forest. *J. Geophys. Res.* 102 (D24), 29205–29212.
- Basu, S., Baker, D.F., Chevallier, F., Patra, P.K., Liu, J., Miller, J.B., 2018. The impact of transport model differences on CO<sub>2</sub> surface flux estimates from OCO-2 retrievals of column average CO<sub>2</sub>. *Atmos. Chem. Phys.* 18 (10), 7189–7215.
- Batchvarova, E., Gryning, S.-E., 1991. Applied model for the growth of the daytime mixed layer. *Boundary Layer Meteorol.* 56 (3), 261–274.
- Behrendt, A., Wulfmeyer, V., Senff, C., Muppa, S.K., Späth, F., Lange, D., Kalhoff, N., Wieser, A., 2020. Observation of sensible and latent heat flux profiles with lidar. *Atmos. Meas. Tech.* 13, 3221–3233.
- Bessonard, G.E.Q., Fosu-Amankwah, K., Petersson, A., Brooks, B.J., 2019. Evaluation of Windsord S1H2 performance in Kumasi during the 2016 DACCIA field campaign. *Atmos. Meas. Tech.* 12, 1311–1324.
- Betts, A.K., 1973. Non-precipitation cumulus convection and its parameterization. *Q. J. R. Meteorol. Soc.* 99, 178–196.
- Betts, A.K., 1992. FIFE atmospheric boundary layer budget methods. *J. Geophys. Res.* 97 (D17), 18523–18531.
- Betts, A.K., 2009. Land-surface-atmosphere coupling in observations and models. *J. Adv. Model. Earth Syst.* 1 (4) <https://doi.org/10.3894/JAMES.2009.1.4>.
- Betts, Alan K., Ball, J.H., 1994. Budget analysis of FIFE 1987 sonde data. *J. Geophys. Res.* 99 (D2), 3655–3666.
- Beets, A.K., Helliker, B., Berry, J., 2004. Coupling between CO<sub>2</sub>, water vapor, temperature, and radon and their fluxes in an idealized equilibrium boundary layer over land. *J. Geophys. Res.* 109, D18103.
- Beyrich, F., 1997. Mixing height estimation from sodar data — a critical discussion. *Atmos. Environ.* 31 (23), 3941–3953.
- Beyrich, F., Leps, J.-P., Mauder, M., Bange, J., Foken, T., Huneke, S., Lohse, H., Lüdi, A., Meijninger, W.M.L., Mironov, D., Weisensee, U., Zittel, P., 2006. Area-averaged surface fluxes over the Litfass region based on eddy-covariance measurements. *Boundary Layer Meteorol.* 121 (1), 33–65.
- Bianco, L., Djalalova, I.V., King, C.W., Wilczak, J.M., 2011. Diurnal evolution and annual variability of boundary-layer height and its correlation to other meteorological variables in California's Central Valley. *Boundary Layer Meteorol.* 140, 491–511.
- Bianco, L., Wilczak, J.M., White, A.B., 2008. Convective boundary layer depth estimation from wind profilers: statistical comparison between an automated algorithm and expert estimations. *J. Atmos. Oceanic Technol.* 25 (8), 1397–1413.
- Blumberg, W.G., Turner, D.D., Löhner, U., Castleberry, S., 2015. Ground-based temperature and humidity profiling using spectral infrared and microwave observations. Part II: Actual retrieval performance in clear-sky and cloudy conditions. *J. Appl. Meteorol. Climatol.* 54, 2305–2319.
- Bonan, G.B., Lawrence, P.J., Oleson, K.W., Lewis, S., Jung, M., Reichstein, M., Lawrence, D.M., Swenson, S.C., 2011. Improving canopy processes in the Community Land Model version 4 (CLM4) using global flux fields empirically inferred from FLUXNET data. *Journal of Geophysical Research: Biogeosciences* 116, G02014.
- Brady, J.M., Stokes, M.D., Bonnardel, J., Bertram, T.H., 2016. Characterization of a quadrotor unmanned aircraft system for aerosol-particle-concentration measurements. *Environ. Sci. Technol.* 50 (3), 1376–1383.
- Brakke, T.W., Verma, S.B., Rosenberg, N.J., 1978. Local and regional components of sensible heat advection. *J. Appl. Meteorol.* (1962–1982) 17 (7), 955–963.
- Brooks, I.A., 2003. Finding boundary layer top: application of a wavelet covariance transform to lidar backscatter profiles. *J. Atmos. Oceanic Technol.* 20, 1092–1105.
- Brugger, P., Banerjee, T., De Roo, F., Kröninger, K., Qubaja, R., Rohatyn, S., Rotenberg, E., Tatarinov, F., Yakir, D., Yang, F., Mauder, M., 2018. Effect of surface heterogeneity on the boundary-layer height: a case study at a semi-arid forest. *Boundary Layer Meteorol.* 169 (2), 233–250.
- Brutsaert, W., 1998. Land-surface water vapor and sensible heat flux: Spatial variability, homogeneity, and measurement scales. *Water Resour. Res.* 34 (10), 2433–2442.
- Brutsaert, W., 1982. *Evaporation into the Atmosphere: Theory, History, and Applications*. Springer, Dordrecht, p. 299.
- Burba, G., 2019. Illustrative maps of past and present eddy covariance measurement locations: II. High-resolution images. Retrieved May 26, 2020, from <https://www.researchgate.net>. 9 pp. doi: 10.13140/RG.2.2.33191.70561.
- Burns, S.P., Blanken, P.D., Turnipseed, A.A., Hu, J., Monson, R.K., 2015. The influence of warm-season precipitation on the diel cycle of the surface energy balance and carbon dioxide at Colorado subalpine forest site. *Biogeosciences* 12, 7349–7377.
- Butterworth, B.J., Desai, A.R., Metzger, S., Townsend, P.A., Schwartz, M.D., Petty, G.W., Mauder, M., Vogelmann, H., Andrenes, C.G., Augustine, T.J., Bertram, T.H., Brown, W.O.J., Buban, M., Cleary, P., Durden, D.J., Florian, C.R., Ruiz, E.G., Iglinaki, T.J., Kruger, E.L., Lantz, K., Lee, T.R., Meyers, T.P., Mineau, J.K., Olson, E.R., Oncley, S.P., Paleri, S., Pertzborn, R.A., Pettersen, C., Plummer, D.M., Riihimaki, L., Sedlar, J., Smith, E.N., Speidel, J., Stoy, P.C., Sühring, M., Thom, J.E., Turner, D.D., Vermeuel, M.P., Wagner, T.J., Wang, Z., Wanner, L., White, L.D., Wilczak, J.M.M., Wright, D.B., Zheng, T., 2021. Connecting land-atmosphere interactions to surface heterogeneity in CHEESEHEAD19. *Bull. Am. Meteorol. Soc.* 102 (2), E421–E445.
- Chen, L., Dirmeyer, P.A., Tawfik, A.B., Lawrence, D.M., 2017. Sensitivities of land cover-precipitation feedback to convective triggering. *J. Hydrometeorol.* 18 (8), 2265–2283.
- Choularton, T.W., Gallagher, M.W., Bower, K.N., Fowler, D., Zahniser, M.S., Kaye, A., Monteith, J.L., Harding, R.J., Fowler, D., Jenkinson, D.S., Monteith, J.L., Unsworth, M.H., 1995. Trace gas flux measurements at the landscape scale using boundary-layer budgets. *Philosoph. Trans. R. Soc. London* 351 (1696), 357–369.
- Chu, H., Baldocchi, D.D., John, R., Wolf, S., Reichstein, M., 2017. Fluxes all of the time? A primer on the temporal representativeness of FLUXNET. *J. Geophys. Res.* 122 (2), 289–307.
- Ciais, P., Rayner, P., Chevallier, F., Bousquet, P., Logan, M., Peylin, P., Ramonet, M., 2010. Atmospheric inversions for estimating CO<sub>2</sub> fluxes: methods and perspectives. In: Jonas, M., Nahorski, Z., Nilsson, S., Whiter, T. (Eds.), *Greenhouse Gas Inventories*. Springer, Dordrecht. [https://doi.org/10.1007/978-94-007-1670-4\\_6](https://doi.org/10.1007/978-94-007-1670-4_6).
- Cleugh, H.A., Grimmond, C.S.B., 2001. Modelling regional scale surface energy exchanges and CBL growth in a heterogeneous, urban-rural landscape. *Boundary Layer Meteorol.* 98 (1), 1–31.
- Collier, N., Hoffman, F.M., Lawrence, D.M., Keppel-Aleks, G., Koven, C.D., Riley, W.J., Mu, M., Randerson, J.T., 2018. The International Land Model Benchmarking (ILAMB) system: design, theory, and implementation. *J. Adv. Model. Earth Syst.* 10, 2731–2754.
- Combe, M., Vilà-Guerau de Arellano, J., Ouwersloot, H.G., Peters, W., 2016. Plant water-stress parameterization determines the strength of land-atmosphere coupling. *Agric. For. Meteorol.* 217, 61–73.
- Compton, J.C., Delgado, R., Berkoff, T.A., Hoff, R.M., 2013. Determination of planetary boundary layer height on short spatial and temporal scales: a demonstration of the covariance wavelet transform in ground-based wind profiler and lidar measurements. *J. Atmos. Oceanic Technol.* 30 (7), 1566–1575.
- Crisp, D., Pollock, H.R., Rosenberg, R., Chapsky, L., Lee, R.A.M., Oyafuse, F.A., Frankenberger, C., O'Dell, C.W., Brueggemann, C.J., Doran, G.B., Eldering, A., Fisher, B.M., Fu, D., Gunson, M.R., Mandrake, L., Osterman, G.B., Schwandner, F.M., Sun, K.,

- Taylor, T.E., Wennberg, P.O., Wunch, D., 2017. The on-orbit performance of the orbiting carbon observatory-2 (OCO-2) instrument and its radiometrically calibrated products. *Atmos. Meas. Tech.* 10 (1), 59–81.
- Crowell, S., Baker, D., Schuh, A., Basu, S., Jacobson, A.R., Chevallier, F., Liu, J., Deng, F., Feng, L., Chatterjee, A., Crisp, D., Eldering, A., Jones, D.B., McKain, K., Miller, J., Nassar, R., Oda, T., O'Dell, C., Palmer, P.I., Schimel, D., Stephens, B., Sweeney, C., 2019. The 2015–2016 carbon cycle as seen from OCO-2 and the global *in situ* network. *Atmos. Chem. Phys.* 19, 9797–9831.
- Gulf, A.D., Fisch, G., Malhi, Y., Nobre, C.A., 1997. The influence of the atmospheric boundary layer on carbon dioxide concentrations over a tropical forest. *Agric. For. Meteorol.* 85, 149–158.
- Davis, K.J., Lenschow, D.H., Oncley, S.P., Kiemle, C., Ehret, G., Giez, A., 1997. The role of entrainment in surface-atmosphere interactions over the boreal forest. *J. Geophys. Res.* 102, 29219–29230.
- Davis, K.J., Gamage, N., Hagelberg, C., Lenschow, D.H., Kiemle, C., Sullivan, P.P., 2000. An objective method for determining atmospheric structure from airborne lidar observations. *J. Atmos. Oceanic Technol.* 17, 1455–1468.
- Davis, K.J., Bakwin, P.S., Berger, B.W., Yi, C., Zhao, C., Teclaw, R.M., Isebrands, J.G., 2003. The annual cycle of CO<sub>2</sub> and H<sub>2</sub>O exchange over a northern mixed forest as observed from a very tall tower. *Global Change Biol.* 9, 1278–1293.
- Davis, K.J., Deng, A., Lauvaux, T., Miles, N.L., Richardson, S.J., Sarmiento, D.P., Gurney, K.R., Hardesty, R.M., Bonin, T.A., Brewer, W.A., Lamb, B.K., Shepson, P.B., Harvey, R.M., Cambaliza, M.O., Sweeney, C., Turnbull, J.C., Whetstone, J., Karion, A., 2017. The Indianapolis flux experiment (INFLUX): a test-bed for developing urban greenhouse gas emission measurements. *Elementa Sci. Anthropocene* 5, 21.
- Davis, K.J., 2008. Integrating field measurements with flux tower and remote sensing data. In: Hoover, Coeli M. (Ed.), *Field Measurements for Landscape-Scale Forest Carbon Monitoring*. Hardcover, p. 20. XVIII, 242 illus ISBN: 978-1-4020-8505-5.
- Davy, R., Esau, I., 2016. Differences in the efficacy of climate forcings explained by variations in atmospheric boundary layer depth. *Nat. Commun.* 7 (1), 11690.
- Deng, A., Lauvaux, T., Davis, K.J., Gaudet, B.J., Miles, N., Richardson, S.J., Wu, K., Sarmiento, D.P., Hardesty, R.M., Bonin, T.A., Brewer, W.A., Gurney, K.R., 2017. Toward reduced transport errors in a high-resolution urban CO<sub>2</sub> inversion system. *Elementa Sci. Anthropocene* 5, 20.
- Denissen, J.M.C., Orth, R., Wouters, H., Miralles, D.G., van Heerwarden, C.C., Vila-Guerau de Arellano, J., Teuling, A.J., 2021. Soil moisture signature in global weather balloon soundings. *npj Clim. Atmosph. Sci.* 4, 13.
- Denmead, O.T., Raupach, M.R., Dunin, F.X., Cleugh, H.A., Leuning, R., 1996. Boundary layer budgets for regional estimates of scalar fluxes. *Global Change Biol.* 2 (3), 255–264.
- Denning, A.S., Zhang, N., Yi, C., Branson, M., Davis, K., Kleist, J., Bakwin, P., 2008. Evaluation of modeled atmospheric boundary layer depth at the WLEF tower. *Agric. For. Meteorol.* 148 (2), 206–215.
- Denning, A.S., Fung, I.Y., Randall, D., 1995. Latitudinal gradient of atmospheric CO<sub>2</sub> due to seasonal exchange with land biota. *Nature* 376 (6537), 240–243.
- Denning, A.S., Takahashi, T., Friedlingstein, P., 1999. Can a strong atmospheric CO<sub>2</sub> rectifier effect be reconciled with a “reasonable” carbon budget? *Tellus B* 51 (2), 249–253.
- Desai, A.R., Davis, K.J., Senff, C., Ismail, S., Browell, E.V., Stauffer, D.R., Reen, B.P., 2005. A case study on the effects of heterogeneous soil moisture on mesoscale boundary layer structure in the southern Great Plains, USA. Part I: simple prognostic model. *Boundary Layer Meteorol.* 120, 275–314.
- Desai, A.R., Helliker, B.R., Moorcroft, P.R., Andrews, A.E., Berry, J.A., 2010. Climatic controls of interannual variability in regional carbon fluxes from top-down and bottom-up perspectives. *J. Geophys. Res.* 115, G02011.
- Desjardins, R.L., Buckley, D.J., Amour, G.St., 1984. Eddy flux measurements of CO<sub>2</sub> above corn using a microcomputer system. *Agric. For. Meteorol.* 32 (3), 257–265.
- De Wekker, S.F.J., Steyn, D.G., Nyeki, S., 2004. A comparison of aerosol-layer and convective boundary-layer structure over a mountain range during Staarte '97. *Boundary Layer Meteorol.* 113, 249–271.
- Díaz-Isaac, L.I., Lauvaux, T., Bocquet, M., Davis, K.J., 2019. Calibration of a multi-physics ensemble for estimating the uncertainty of a greenhouse gas atmospheric transport model. *Atmos. Chem. Phys.* 19, 5695–5718.
- Díaz-Isaac, L.I., Lauvaux, T., Davis, K.J., 2018. Impact of physical parameterizations and initial conditions on simulated atmospheric transport and CO<sub>2</sub> mole fractions in the US Midwest. *Atmos. Chem. Phys.* 18, 14813–14835.
- Driedonks, A.G.M., Tennekes, H., 1984. Entrainment effects in the well-mixed atmospheric boundary layer. *Boundary Layer Meteorol.* 30 (1), 75–105.
- Durre, I., Vose, R.S., Wuertz, D.B., 2006. Overview of the integrated global radiosonde archive. *J. Clim.* 19 (1), 53–68.
- Eder, F., Schmidt, M., Damian, T., Träumner, K., Mauder, M., 2015a. Mesoscale eddies affect near-surface turbulent exchange: evidence from lidar and tower measurements. *J. Appl. Meteorol. Climatol.* 54 (1), 189–206.
- Eder, F., De Roo, F., Rotenberg, E., Yakir, D., Schmid, H.P., Mauder, M., 2015b. Secondary circulations at a solitary forest surrounded by semi-arid shrubland and their impact on eddy-covariance measurements. *Agric. For. Meteorol.* 211–212, 115–127.
- Edwards, J.M., Beljaars, A.C.M., Holtslag, A.A.M., Lock, A.P., 2020. Representation of boundary-layer processes in numerical weather prediction and climate models. *Boundary Layer Meteorol.* 177, 511–539.
- El-Madany, T.S., Duarte, H.F., Durden, D.J., Paas, B., Deventer, M.J., Juang, J.-Y., Leclerc, M.Y., Klemm, O., 2014. Low-level jets and above-canopy drainage as causes of turbulent exchange in the nocturnal boundary layer. *Biogeosciences* 11, 4507–4519.
- Ek, M.B., Holtslag, A.A.M., 2004. Influence of soil moisture on boundary layer cloud development. *J. Hydrometeorol.* 5 (1), 86–99.
- Emeis, S., Münkel, C., Vogt, S., Müller, W.J., Schäfer, K., 2004. Atmospheric boundary-layer structure from simultaneous SODAR, RASS, and ceilometer measurements. *Atmos. Environ.* 38 (2), 273–286.
- Eresmaa, N., Karppinen, A., Joffre, S.M., Räsänen, J., Talvitie, H., 2006. Mixing height determination by ceilometer. *Atmos. Chem. Phys.* 6, 1485–1493.
- Feng, S., Lauvaux, T., Keller, K., Davis, K.J., Rayner, P., Oda, T., Gurney, K.R., 2019. A road map for improving the treatment of uncertainties in high-resolution regional carbon flux inverse estimates. *Geophys. Res. Lett.* 46, 13461–13469.
- Feng, S., Lauvaux, T., Davis, K.J., Keller, K., Zhou, Y., Williams, C., Schuh, A., Liu, J., Baker, I., 2020. Seasonal characteristics of model uncertainties from biogenic fluxes, transport, and large-scale boundary inflow in atmospheric CO<sub>2</sub> simulations over North America. *J. Geophys. Res.* 124, 14325–14346.
- Findell, K.L., Eltahir, E.A.B., 2003a. Atmospheric controls on soil moisture-boundary layer interactions. Part I: framework development. *J. Hydrometeorol.* 4 (3), 552–569.
- Findell, K.L., Eltahir, E.A.B., 2003b. Atmospheric controls on soil moisture-boundary layer interactions. Part II: feedbacks within the continental United States. *J. Hydrometeorol.* 4 (3), 570–583.
- Ford, T.W., Quiring, S.M., Frauenfeld, O.W., Rapp, A.D., 2015. Synoptic conditions related to soil moisture-atmosphere interactions and unorganized convection in Oklahoma. *J. Geophys. Res.* 120 (22), 519–535.
- Gentine, P., Chhang, A., Rigden, A., Salvucci, G., 2016. Evaporation estimates using weather station data and boundary layer theory. *Geophys. Res. Lett.* 43 (22), 661–670.
- Gentine, Pierre, Ferguson, C.R., Holtslag, A.A.M., 2013a. Diagnosing evaporative fraction over land from boundary-layer clouds. *J. Geophys. Res.* 118 (15), 8185–8196.
- Gerken, T., Bromley, G.T., Stoy, P.C., 2018a. Surface moistening trends in the northern North American great plains increase the likelihood of convective initiation. *J. Hydrometeorol.* 19 (1), 227–244.
- Gentine, Pierre, Holtslag, A.A.M., D'Andrea, F., Ek, M., 2013b. Surface and atmospheric controls on the onset of moist convection over land. *J. Hydrometeorol.* 14 (5), 1443–1462.
- Gerken, T., Bromley, G.T., Ruddell, B.L., Williams, S., Stoy, P.C., 2018b. Convective suppression before and during the United States Northern Great Plains flash drought of 2017. *Hydrocl. Earth Syst. Sci.* 22, 4155–4163.
- Gerken, T., Ruddell, B.L., Yu, R., Stoy, P.C., Drewry, D.T., 2019. Robust observations of land-to-atmosphere feedbacks using the information flows of FLUXNET. *npj Climate Atmosph. Sci.* 2 (1), 37.
- Gibert, F., Koch, G.J., Beyon, J.Y., Hilton, T.W., Davis, K.J., Andrews, A., Flamant, P.H., Singh, U.N., 2011. Can CO<sub>2</sub> turbulent flux measurements be made by lidar? A preliminary study. *J. Atmos. Oceanic Technol.* 28, 365–377.
- Grant, L.D., van den Heever, S.C., 2016. Cold pool dissipation. *J. Geophys. Res.* 121 (3), 1138–1155.
- Green, J.K., Seneviratne, S.I., Berg, A.M., Findell, K.L., Hagemann, S., Lawrence, D.M., Gentine, P., 2019. Large influence of soil moisture on long-term terrestrial carbon uptake. *Nature* 565 (7740), 476–479.
- Griebel, A., Bennett, L.T., Metzen, D., Cleverly, J., Burba, G., Arndt, S.K., 2016. Effects of inhomogeneities within the flux footprint on the interpretation of seasonal, annual, and interannual ecosystem carbon exchange. *Agric. For. Meteorol.* 221, 50–60.
- Griffis, T.J., Zhang, J., Baker, J.M., Kljun, N., Billmark, K., 2007. Determining carbon isotope signatures from micrometeorological measurements: Implications for studying biosphere-atmosphere exchange processes. *Boundary Layer Meteorol.* 123 (2), 295–316.
- Grimsdell, A.W., Angevine, W.M., 1998. Convective boundary layer height Measurement with wind profilers and comparison to cloud base. *J. Atmos. Oceanic Technol.* 15, 1331–1338.
- Grund, C.J., Banta, R.M., George, J.L., Howell, J.N., Post, M.J., Richter, R.A., Weickmann, A.M., 2001. High-resolution doppler lidar for boundary layer and cloud research. *J. Atmos. Oceanic Technol.* 18 (3), 376–393.
- Gustafson, W.L., Vogelman, A.M., Li, Z., Cheng, X., Dumas, K.K., Endo, S., Johnson, K.L., Krishna, B., Toto, T., Xiao, H., 2020. The Large-Eddy Simulation (LES) atmospheric radiation measurement (ARM) symbiotic simulation and observation (LASSO) activity for continental shallow convection. *Bull. Am. Meteorol. Soc.* 101, E462–E479.
- Hammerle, A., Haslwanter, A., Schmitt, M., Bahn, M., Tappeiner, U., Cernusca, A., Wohlfahrt, G., 2007. Eddy covariance measurements of carbon dioxide, latent and sensible energy fluxes above a meadow on a mountain slope. *Boundary Layer Meteorol.* 122, 397–416.
- Harman, I.N., Finnigan, J.J., 2007. A simple unified theory for flow in the canopy and roughness sublayer. *Boundary Layer Meteorol.* 123, 339–363.
- Harman, I.N., Finnigan, J.J., 2008. Scalar concentration profiles in the canopy and roughness sublayer. *Boundary Layer Meteorol.* 129, 323–351.
- Hartery, S., Commane, R., Lindaas, J., Sweeney, C., Henderson, J., Mountain, M., Steiner, N., McDonald, K., Dinardo, S.J., Miller, C.E., Wofsy, S.C., Chang, R.Y.-W., 2018. Estimating regional-scale methane flux and budgets using CARVE aircraft measurements over Alaska. *Atmos. Chem. Phys.* 18 (1), 185–202.
- Hicks, B., Martin, H., 1972. Atmospheric turbulent fluxes over snow. *Boundary Layer Meteorol.* 2, 496–502.
- Hiller, R., Zeeman, M.J., Eugster, W., 2008. Eddy-covariance flux measurements in the complex terrain of an alpine valley in Switzerland. *Boundary Layer Meteorol.* 127, 449–467.
- Heinsch, F.A., Zhao, M., Running, S.W., Kimball, J.S., Nemani, R.R., Davis, K.J., Bolstad, P.V., Cook, B.D., Desai, A.R., Ricciuto, D.M., Law, B.E., Oechel, W.C.,

- Kwon, H., Luo, H., Wofsy, S.C., Dunn, A.L., Munger, J.W., Baldocchi, D.D., Xu, L., Hollinger, D.Y., Richardson, A.D., Stoy, P.C., Siqueira, M.B.S., Monson, R.K., Burns, S., Flanagan, L.B., 2006. Evaluation of remote sensing based terrestrial productivity from MODIS using regional tower eddy flux network observations. *IEEE Trans. Geosci. Remote Sens.* 44, 1908–1925.
- Helbig, M., Waddington, J.M., Alekseychik, P., Amiro, B.D., Aurela, M., Barr, A.G., Black, T.A., Carey, S.K., Chen, J., Chi, J., Desai, A.R., Dunn, A., Euskirchen, E.S., Flanagan, L.B., Friborg, T., Garneau, M., Grelle, A., Harder, S., Heliasz, M., Humphreys, E.R., Ikawa, H., Isabelle, P.-E., Iwata, H., Jassal, R., Korkiakoski, M., Kurbatova, J., Kutzbach, L., Lapshina, E., Lindroth, A.M., Löfvenius, M.O., Lohila, A., Mammarella, I., Marsh, P., Moore, P.A., Maximov, T., Nadeau, D.F., Nicholls, E.M., Nilsson, M.B., Ohta, T., Peichl, M., Petrone, R.M., Prokushkin, A., Quinton, W.L., Roulet, N.T., Runkle, B.R.K., Sonnentag, O., Strachan, I.B., Taillardat, P., Tuittila, E.-S., Tuovinen, J.-P., Turner, J., Ueyama, M., Varlagin, A., Vesala, T., Wilming, M., Zyrianov, V., 2020a. The biophysical climate mitigation potential of boreal peatlands during the growing season. *Environ. Res. Lett.* 15, 104004.
- Helbig, M., Waddington, J.M., Alekseychik, P., Amiro, B.D., Aurela, M., Barr, A.G., Black, T.A., Blanken, P.D., Carey, S.K., Chen, J., Chi, J., Desai, A.R., Dunn, A., Euskirchen, E.S., Flanagan, L.B., Forbrich, I., Friborg, T., Grelle, A., Harder, S., Heliasz, M., Humphreys, E.R., Ikawa, H., Isabelle, P.-E., Iwata, H., Jassal, R., Korkiakoski, M., Kurbatova, J., Kutzbach, L., Lindroth, A.M., Löfvenius, M.O., Lohila, A., Mammarella, I., Marsh, P., Maximov, T., Melton, J.R., Moore, P.A., Nadeau, D.F., Nicholls, E.M., Nilsson, M.B., Ohta, T., Peichl, M., Petrone, R.M., Petrov, R., Prokushkin, A., Quinton, W.L., Roulet, N.T., Runkle, B.R.K., Sonnentag, O., Strachan, I.B., Taillardat, P., Tuittila, E.-S., Tuovinen, J.-P., Turner, J., Ueyama, M., Varlagin, A., Wilming, M., Wofsy, S.C., Zyrianov, V., 2020b. Increasing contribution of peatlands to boreal evapotranspiration in a warming climate. *Nature Clim. Change* 10, 555–560.
- Helbig, M., Wischnewski, K., Kljun, N., Chasmer, L.E., Quinton, W.L., Dettò, M., Sonnentag, O., 2016. Regional atmospheric cooling and wetting effect of permafrost thaw-induced boreal forest loss. *Global Change Biol.* 22 (12), 4048–4066.
- Helliker, B.R., Berry, J.A., Betts, A.K., Bakwin, P.S., Davis, K.J., Denning, A.S., Ehleringer, J.R., Miller, J.B., Butler, M.P., Ricciuto, D.M., 2004. Estimates of net CO<sub>2</sub> flux by application of equilibrium boundary layer concepts to CO<sub>2</sub> and water vapor measurements from a tall tower. *J. Geophys. Res.* 109, D20106.
- Hemes, K.S., Eichelmann, E., Chamberlain, S.D., Knox, S.H., Oikawa, P.Y., Sturtevant, C., Verfaillie, J., Szutu, D., Baldocchi, D.D., 2018. A unique combination of aerodynamic and surface properties contribute to surface cooling in restored wetlands of the Sacramento-San Joaquin Delta, California. *J. Geophys. Res.* 123 (7), 2072–2090.
- Hilton, T.W., Davis, K.J., Keller, K., 2014. Evaluating terrestrial CO<sub>2</sub> flux diagnoses and uncertainties from a simple land surface model and its residuals. *Biogeosciences* 11, 217–235.
- Hu, X.-M., Nielsen-Gammon, J.W., Zhang, F., 2010. Evaluation of three planetary boundary layer schemes in the WRF model. *J. Appl. Meteorol. Climatol.* 49 (9), 1831–1844.
- Hu, L., Andrews, A.E., Thoning, K.W., Sweeney, C., Miller, J.B., Michalak, A.M., Drlugokencky, E., Tans, P.P., Shiga, Y.P., Mountain, M., Nehrkorn, T., Montzka, S.A., McKain, K., Koffler, J., Trudeau, M., Michel, S.E., Biraud, S.C., Fischer, M.L., Worthy, D.E.J., Vaughn, B.H., White, J.W.C., Yadav, V., Basu, S., van der Velde, I.R., 2019. Enhanced North American carbon uptake associated with El Niño. *Sci. Adv.* 5 (6), eaaw0076.
- Humphrey, V., Berg, A., Ciais, P., Gentile, P., Jung, M., Reichstein, M., Seneviratne, S.I., Frankenberger, C., 2021. Soil moisture-atmosphere feedback dominates land carbon uptake variability. *Nature* 592, 65–69.
- Janssen, R.H.H., Vilà-Guerau de Arellano, J., Jimenez, J.L., Ganzeveld, L.N., Robinson, N.H., Allan, J.D., Coe, H., Pugh, T.A.M., 2013. Influence of boundary layer dynamics and isoprene chemistry on the organic aerosol budget in a tropical forest. *J. Geophys. Res.* 118 (16), 9351–9366.
- Juang, J.-Y., Katul, G.G., Porporato, A., Stoy, P.C., Siqueira, M.S., Dettò, M., Kim, H.-S., Oren, R., 2007a. Eco-hydrological controls on summertime convective rainfall triggers. *Global Change Biol.* 13, 887–896.
- Juang, J.-Y., Porporato, A., Stoy, P.C., Siqueira, M.S., Oishi, A.C., Dettò, M., Kim, H.-S., Katul, G.G., 2007b. Hydrologic and atmospheric controls on initiation of convective precipitation events. *Water Resour. Res.* 43, WR004954.
- Jung, M., Reichstein, M., Margolis, H.A., Cescatti, A., Richardson, A.D., Arain, M.A., Arneth, A., Bernhofer, C., Bonal, D., Chen, J., Gianelle, D., Gobron, N., Kiely, G., Kutsch, W., Lasslop, G., Law, B.E., Lindroth, A., Merbold, L., Montagnani, L., Moors, E.J., Papale, D., Sottocornola, M., Vaccari, F., Williams, C., 2011. Global patterns of land-atmosphere fluxes of carbon dioxide, latent heat, and sensible heat derived from eddy covariance, satellite, and meteorological observations. *J. Geophys. Res.* 116, G00J07.
- Kaimal, J.C., Wyngaard, J.C., 1990. The Kansas and Minnesota experiments. *Boundary Layer Meteorol.* 50, 31–47.
- Kang, S., Davis, K.J., LeMone, M.A., 2007. Observations of the ABL structures over a heterogeneous land surface during IHOP 2002. *J. Hydrometeorol.* 8, 221–244.
- Karipot, A., Leclerc, M.Y., Zhang, G., Martin, T., Starr, G., Hollinger, D., McCaughey, J.H., Hendrey, G.R., 2006. Nocturnal CO<sub>2</sub> exchange over a tall forest canopy associated with intermittent low-level jet activity. *Theor. Appl. Climatol.* 85, 243–248.
- Keenan, T.F., Hollinger, D.Y., Bohrer, G., Dragoni, D., Munger, J.W., Schmid, H.P., Richardson, A.D., 2013. Increase in forest water-use efficiency as atmospheric carbon dioxide concentrations rise. *Nature* 499 (7458), 324–327.
- Keenan, T.F., Moore, D.J.P., Desai, A., 2019. Growth and opportunities in networked synthesis through AmeriFlux. *New Phytol.* 222 (4), 1685–1687.
- Kiemle, C., Brewer, W.A., Ehret, G., Hardesty, R.M., Fix, A., Senff, C., Wirth, M., Poheraj, G., LeMone, M.A., 2007. Latent heat flux profiles from colocated airborne water vapor and wind lidars during IHOP\_2002. *J. Atmos. Oceanic Technol.* 24, 627–639.
- Kiese, R., Fersch, B., Baessler, C., Brosy, C., Butterbach-Bahl, K., Chwala, C., Dannenmann, M., Fu, J., Gasche, R., Grote, R., Jahn, C., Klatt, J., Kunstmann, H., Mauder, M., Rödiger, T., Smiatek, G., Soltau, M., Steinbrecher, R., Völksch, I., Schmid, H.P., 2018. The TERENO pre-alpine observatory: integrating meteorological, hydrological, and biogeochemical measurements and modeling. *Vadose Zone J.* 17 (1), 180060.
- Kljun, N., Rotach, M.W., Schmid, H.P., 2002. A 3D backward Lagrangian footprint model for a wide range of boundary layer stratifications. *Boundary Layer Meteorol.* 103, 205–226.
- Kljun, N., Calanca, P., Rotach, M.W., Schmid, H.P., 2015. A simple two-dimensional parameterisation for Flux Footprint Prediction (FFP). *Geosci. Model Devel.* 8 (11), 3695–3713.
- Knohl, A., Baldocchi, D.D., 2008. Effects of diffuse radiation on canopy gas exchange processes in a forest ecosystem. *J. Geophys. Res.* 113, G02023.
- Knox, S.H., Jackson, R.B., Poultier, B., McNicol, G., Fluet-Chouinard, E., Zhang, Z., Hugelius, G., Bousquet, P., Canadel, J.G., Saunois, M., Papale, D., Chu, H., Keenan, T.F., Baldocchi, D., Torn, M.S., Mammarella, I., Trott, C., Aurela, M., Bohrer, G., Zona, D., 2019. FLUXNET-CH4 synthesis activity: objectives, observations, and future directions. *Bull. Am. Meteorol. Soc.* 100, 2607–2632.
- Konings, A.G., Katul, G.G., Porporato, A., 2010. The rainfall-no rainfall transition in a coupled land-convective atmosphere system. *Geophys. Res. Lett.* 37, L14401.
- Koster, R.D., Schubert, S.D., Suarez, M.J., 2009. Analyzing the concurrence of meteorological droughts and warm periods, with implications for the determination of evaporative regime. *J. Climate* 22 (12), 3331–3341.
- Kotthaus, S., Grimmond, C.S.B., 2018a. Atmospheric boundary-layer characteristics from ceilometer measurements. Part 1: a new method to track mixed layer height and classify clouds. *Q. J. R. Meteorol. Soc.* 144 (714), 1525–1538.
- Kotthaus, S., Grimmond, C.S.B., 2018b. Atmospheric boundary-layer characteristics from ceilometer measurements. Part 2: application to London's urban boundary layer. *Q. J. R. Meteorol. Soc.* 144 (714), 1511–1524.
- Kotthaus, S., Halios, C., Barlow, F.J., Grimmond, C.S.B., 2018. Volume for pollution dispersion: London's atmospheric boundary layer during ClearLo observed with two ground-based lidar types. *Atmos. Environ.* 190, 401–414.
- Kröniger, K., De Roo, F., Brugge, P., Huq, S., Banerjee, T., Zinsser, J., Rotenberg, E., Yakir, D., Rohatyn, S., Mauder, M., 2018. Effect of secondary circulations on the surface-atmosphere exchange of energy at an isolated semi-arid forest. *Boundary Layer Meteorol.* 169 (2), 209–232.
- Kutter, E., Yi, C., Hendrey, G., Liu, H., Eaton, T., Ni-Meister, W., 2017. Recirculation over complex terrain. *J. Geophys. Res.-Atmosph.* 122, 6637–6651.
- Kuze, A., Suto, H., Shioimi, K., Kawakami, S., Tanaka, M., Ueda, Y., Deguchi, A., Yoshida, J., Yamamoto, Y., Kataoka, F., Taylor, T.E., Buijs, H.L., 2016. Update on GOSAT TANSO-FTS performance, operations, and data products after more than 6 years in space. *Atmos. Meas. Tech.* 9 (6), 2445–2461.
- Lang, A.R.G., Evans, G.N., Ho, P.Y., 1974. The influence of local advection on evapotranspiration from irrigated rice in a semi-arid region. *Agricul. Meteorol.* 13 (1), 5–13.
- Lang, A.R.G., McNaughton, K.G., Fazu, C., Bradley, E.F., Ohtaki, E., 1983. An experimental appraisal of the terms in the heat and moisture flux equations for local advection. *Boundary Layer Meteorol.* 25 (1), 89–102.
- Lansu, E.M., van Heerwaarden, C.C., Stegehuis, A.I., Teuling, A.J., 2020. Atmospheric aridity and apparent soil moisture drought in European forest during heat waves. *Geophys. Res. Lett.* 47 (6), e2020GL087091.
- Lauvaux, T., Miles, N.L., Deng, A., Richardson, S.J., Cambaliza, M.O., Davis, K.J., Gaudet, B., Gurney, K.R., Huang, J., O'Keeffe, D., Song, Y., Karion, A., Oda, T., Patarasuk, R., Sarmiento, D., Shepson, P., Sweeney, C., Turnbull, J., Wu, K., 2016. High resolution atmospheric inversion of urban CO<sub>2</sub> emissions during the dormant season of the Indianapolis Flux Experiment (INFLUX). *J. Geophys. Res. Atmosph.* 121, 5213–5236.
- Lauvaux, T., Davis, K.J., 2014. Planetary boundary layer errors in mesoscale inversions of column-integrated CO<sub>2</sub> measurements. *J. Geophys. Res.* 119 (2), 490–508.
- Lauvaux, T., Schuh, A.E., Ulasz, M., Richardson, S., Miles, N., Andrews, A.E., Sweeney, C., Diaz, L.I., Martins, D., Shepson, P., Bove, K.J., 2012. Constraining the CO<sub>2</sub> budget of the corn belt: exploring uncertainties from the assumptions in a mesoscale inverse system. *Atmos. Chem. Phys.* 12, 337–354.
- Lee, X., Goulden, M., Hollinger, D.Y., Barr, A., Black, T.A., Bohrer, G., Bracho, R., Drake, B., Goldstein, A., Gu, L., Katul, G., Kolb, T., Law, B.E., Margolis, H., Meyers, T., Monson, R., Munger, W., Oren, R., Paw, U.K.T., Richardson, A.D., Schmid, H.P., Staebler, R., Wofsy, S., Zhao, L., 2011. Observed increase in local cooling effect of deforestation at higher latitudes. *Nature* 479, 384–387.
- Lehner, M., Rotach, M.W., 2018. Current challenges in understanding and predicting transport and exchange in the atmosphere over mountainous terrain. *Atmosphere* 9, 276.
- Leuning, R., Denmead, O.T., Lang, A.R.G., Ohtaki, E., 1982. Effects of heat and water vapor transport on eddy covariance measurement of CO<sub>2</sub> fluxes. *Boundary Layer Meteorol.* 23 (2), 209–222.
- Löhner, U., Turner, D.D., Crewell, S., 2009. Ground-based temperature and humidity profiling using spectral infrared and microwave observations. Part I: simulated retrieval performance in clear-sky conditions. *J. Appl. Meteor. Climatol.* 48, 1017–1032.
- Lotterer, C., Piringer, M., 2016. Mixing-height time series from operational ceilometer aerosol-layer heights. *Boundary Layer Meteorol.* 161, 265–287.

- Luyssaert, S., Jammet, M., Stoy, P.C., Estel, S., Pongratz, J., Ceschia, E., Churkina, G., Don, A., Erb, K., Ferlicq, M., Gielen, B., Grünwald, T., Houghton, R.A., Klumpp, K., Knoblauch, A., Kolb, T., Kuemmerle, T., Laurila, T., Lohila, A., Dolman, A.J., 2014. Land management and land-cover change have impacts of similar magnitude on surface temperature. *Nature Climate Change* 4 (5), 389–393.
- Mahrt, L., 2000. Surface heterogeneity and vertical structure of the boundary layer. *Boundary Layer Meteorol.* 96, 33–62.
- Mahrt, L., 1999. Stratified atmospheric boundary layers. *Boundary Layer Meteorol.* 90, 375–396.
- Manoli, G., Domec, J.-C., Novick, K., Oishi, A.C., Noormets, A., Marani, M., Katul, G., 2016. Soil-plant-atmosphere conditions regulating convective cloud formation above southeastern US pine plantations. *Global Change Biol.* 22 (6), 2238–2254.
- Mauder, M., Foken, T., Cuxart, J., 2020. Surface-energy-balance closure over land: a review. *Boundary Layer Meteorol.* <https://doi.org/10.1007/s10546-020-00529-6>.
- McColl, K.A., Ridgen, A.J., 2020. Emergent simplicity of continental evapotranspiration. *Geophys. Res. Lett.* 47 (6), e2020GL087101.
- McGrath-Spangler, E.L., Molod, A., Ott, L.E., Pawson, S., 2015. Impact of planetary boundary layer turbulence on model climate and tracer transport. *Atmos. Chem. Phys.* 15 (13), 7269–7286.
- McKee, D.C., Thurtell, G.W., 1978. Measurements of energy fluxes involved in energy budget of a snow cover. *J. Appl. Meteorol.* 17, 339–349.
- McNaughton, K.G., Spriggs, T.W., 1986. A mixed-layer model for regional evaporation. *Boundary Layer Meteorol.* 34 (3), 243–262.
- Mechem, D.B., Kogan, Y.L., Schultz, D.M., 2010. Large-eddy observation of post-cold-frontal continental stratocumulus. *J. Atmospheric Sci.* 67, 3368–3383.
- Meijninger, W.M.L., Hartogensis, O.K., Kohsieck, W., Hoedjes, J.C.B., Zuurbier, R.M., De Bruin, H.A.R., 2002. Determination of area-averaged sensible heat fluxes with a large aperture scintillometer over a heterogeneous surface – Flevoland Field Experiment. *Boundary Layer Meteorol.* 105, 37–62.
- Menke, R., Vasiljević, N., Mann, J., Lundquist, J.K., 2019. Characterization of flow recirculation zones at the Perdigão site using multi-lidar measurements. *Atmosph. Chem. Phys.* 19, 2713–2723.
- Miles, N.L., Richardson, S.J., Davis, K.J., Lauvaux, T., Andrews, A.E., West, T.O., Bandaru, V., Crosson, E.R., 2012. Large amplitude spatial and temporal gradients in atmospheric boundary layer CO<sub>2</sub> mole fractions detected with a tower-based network in the U.S. upper Midwest. *J. Geophys. Res.* 117, G01019.
- Miralles, D.G., Gentile, P., Seneviratne, S.I., Teuling, A.J., 2019. Land-atmospheric feedbacks during droughts and heatwaves: state of the science and current challenges: Land feedbacks during droughts and heatwaves. *Ann. N. Y. Acad. Sci.* 1436 (1), 19–35.
- Miralles, D.G., Teuling, A.J., van Heerwaarden, C.C., Vilà-Guerau de Arellano, J., 2014. Mega-heatwave temperatures due to combined soil desiccation and atmospheric heat accumulation. *Nat. Geosci.* 7 (5), 345–349.
- Molod, A., Salmon, H., Dempsey, M., 2015. Estimating planetary boundary layer heights from NOAA Profiler Network Wind Profiler data. *J. Atmos. Oceanic Technol.* 32 (9), 1545–1561.
- Monin, A.S., Obukhov, A.M., 1954. Osnovnye zakonomernosti turbulentnogo peremeshivaniya v prizmennom sloe atmosfery (Basic Laws of Turbulent Mixing in the Atmosphere Near the Ground). Trudy geofiz. inst. AN SSSR 24 (151), 163–187.
- Myrup, L.O., Morgan, D.L., Boomer, R.L., 1982. Summertime three-dimensional wind field above Sacramento, California. *J. Clim. Appl. Meteorol.* 22, 256–265.
- National Academies of Sciences, Engineering, and Medicine, 2018. Thriving on our Changing Planet: A Decadal Strategy for Earth Observation from Space. The National Academies Press, Washington, DC. <https://doi.org/10.17226/24938>.
- NCAR/EOL In-situ Sensing Facility, 2020. NCAR/EOL ISS Ceilometer Data and High-Rate ISFS surface flux data, tilt corrected, geographic coordinate winds and ISS Radiosonde Data and ISS 449 MHz Radar Wind Profiler, 5 and 30 Minute Winds. Versions 1.0. UCAR/NCAR - Earth Observing Laboratory <https://doi.org/10.26023/W3XH-2KYX-2C01>. Accessed 10 Apr 2020.
- Neggers, R.A.J., Siebesma, A.P., Heus, T., 2012. Continuous single-column model evaluation at a permanent meteorological supersite. *Bull. Am. Meteorol. Soc.* 93 (9), 1389–1400.
- Newsom, R.K., Turner, D.D., Lehtinen, R., Müinkel, C., Kallio, J., Roininen, R., 2020. Evaluation of a compact broadband differential absorption lidar for routine water vapor profiling in the atmospheric boundary layer. *J. Atmos. Oceanic Technol.* 37, 47–65.
- Niyogi, D., Alapaty, K., Booker, F., Chen, F., Davis, K.J., Holben, B., Matsui, T., Meyers, T., Oechel, W.C., Pielke Sr., R.A., Wells, R., Wilson, K., Xue, Y., Chang, H.-I., Saxena, V.K., Holt, T., 2004. Direct observations of the effects of aerosol loading on net ecosystem CO<sub>2</sub> exchanges over different landscapes. *Geophys. Res. Lett.* 31, L20506.
- Niu, S., Luo, Y., Fei, S., Yuan, W., Schimel, D., Law, B.E., Ammann, C., Arain, M.A., Arneth, A., Aubinet, M., Barr, A., Beringer, J., Bernhofer, C., Black, T.A., Buchmann, N., Cescatti, A., Chen, J., Davis, K.J., Dellwik, E., Zhou, X., 2012. Thermal optimality of net ecosystem exchange of carbon dioxide and underlying mechanisms. *New Phytol.* 194 (3), 775–783.
- Novick, K.A., Biederman, J.A., Desai, A.R., Litvak, M.E., Moore, D.J.P., Scott, R.L., Torn, M.S., 2018. The AmeriFlux network: a coalition of the willing. *Agric. For. Meteorol.* 249, 444–456.
- Novick, K.A., Ficklin, D.L., Stoy, P.C., Williams, C.A., Bohrer, G., Oishi, A.C., Papuga, S.A., Blanken, P.D., Noormets, A., Sulman, B.N., Scott, R.L., Wang, L., Phillips, R.P., 2016. The increasing importance of atmospheric demand for ecosystem water and carbon fluxes. *Nature Climate Change* 6 (11), 1023–1027.
- Novick, K.A., Katul, G.G., 2020. The duality of reforestation impacts on surface and air temperature. *J. Geophys. Res.* 125 (4), e2019JG005543.
- Pal, S., Davis, K.J., Lauvaux, T., Browell, E.V., Gaudet, B.J., Stauffer, D.R., Obland, M.D., Choi, Y., DiGangi, J.P., Feng, S., Lin, B., Miles, N.L., Pauly, R.M., Richardson, S.J., Zhang, F., 2020. Observations of greenhouse gas changes across summer frontal boundaries in the eastern United States. *J. Geophys. Res.* 125, e2019JD030526.
- Panwar, A., Kleidon, A., Renner, M., 2019. Do surface and air temperatures contain similar imprints of evaporative conditions? *Geophys. Res. Lett.* 46 (7), 3802–3809.
- Pastorello, G.Z., et al., 2020. The FLUXNET2015 dataset and the ONEFlux processing pipeline for eddy covariance data. *Sci. Data* 7, 225.
- Patton, E.G., Sullivan, P.P., Shaw, R.H., Finnigan, J.J., Weil, J.C., 2016. Atmospheric stability influences on coupled boundary layer and canopy turbulence. *J. Atmospheric Sci.* 73 (4), 1621–1647.
- Pedruzo-Bagazgoitia, X., Ouwersloot, H.G., Sikma, M., van Heerwaarden, C.C., Jacobs, C.M.J., Vilà-Guerau de Arellano, J., 2017. Direct and diffuse radiation in the shallow cumulus-vegetation system: enhanced and decreased evapotranspiration regimes. *J. Hydrometeorol.* 18 (6), 1731–1748.
- Peylin, P., Law, R.M., Gurney, K.R., Chevallier, F., Jacobson, A.R., Maki, T., Niwa, Y., Patra, P.K., Peters, W., Rayner, P.J., Rödenbeck, C., van der Laan-Luijkx, I.T., Zhnag, X., 2013. Global atmospheric carbon budget: Results from an ensemble of atmospheric CO<sub>2</sub> inversions. *Biogeosciences* 10 (10), 6699–6720.
- Pietersen, H.P., Vilà-Guerau de Arellano, J., Augustin, P., van de Boer, A., de Coster, O., Delbarre, H., Durand, P., Fourmentin, M., Gioli, B., Hartogensis, O., Louhou, F., Lothon, M., Ouwersloot, H.G., Pino, D., Reuder, J., 2015. Study of a prototypical convective boundary layer observed during BLLAST: contributions by large-scale forcings. *Atmos. Chem. Phys.* 15, 4241–4257.
- Pino, D., Vilà-Guerau de Arellano, J., Peters, W., Schröter, J., van Heerwaarden, C.C., Krol, M.C., 2012. A conceptual framework to quantify the influence of convective boundary layer development on carbon dioxide mixing ratios. *Atmos. Chem. Phys.* 12, 2969–2985.
- Prabha, T.V., Leclerc, M.Y., Karipot, A., Hollinger, D.Y., Mursch-Radlgruber, E., 2008. Influence of nocturnal low-level jets on eddy-covariance fluxes over a tall forest canopy. *Boundary Layer Meteorol.* 126 (2), 219–236.
- Priestley, C.H.B., Taylor, R.J., 1972. On the assessment of surface heat flux and evaporation using large-scale parameters. *Monthly Weather Rev.* 100 (2), 81–92.
- Raupach, M.R., 1998. Influences of local feedbacks on land-air exchanges of energy and carbon. *Global Change Biol.* 4 (5), 477–494.
- Raupach, M.R., 2000. Equilibrium evaporation and the convective boundary layer. *Boundary Layer Meteorol.* 96 (1), 107–142.
- Raupach, M.R., 2001. Combination theory and equilibrium evaporation. *Q. J. R. Meteorol. Soc.* 127 (574), 1149–1181.
- Raupach, M.R., Denmead, O.T., Dunin, F.X., 1992. Challenges in linking atmospheric CO<sub>2</sub> concentrations to fluxes at local and regional scales. *Aust. J. Bot.* 40 (5), 697–716.
- Raupach, M.R., Antonia, R.A., Rajagopalan, S., 1991. Rough-wall turbulent boundary layers. *Appl. Mech. Rev.* 44 (1), 1–25.
- Raupach, M.R., Thom, A.S., 1981. Turbulence in and above plant canopies. *Annu. Rev. Fluid Mech.* 13 (1), 97–129.
- Reen, B.P., Stauffer, D.R., Davis, K.J., 2014. Land-surface heterogeneity effects in the planetary boundary layer. *Boundary Layer Meteorol.* 150, 1–31.
- Reen, B.P., Stauffer, D.R., Davis, K.J., Desai, A.R., 2006. A case study on the effects of heterogeneous soil moisture on mesoscale boundary layer structure in the southern Great Plains, USA. Part II: application of a mesoscale numerical weather model. *Boundary Layer Meteorol.* 120, 275–314.
- Rey-Sánchez, C., Wharton, S., Vilà-Guerau de Arellano, J., Paw, U.K.T., Hemes, K.S., Fuentes, J.D., Osuna, J., Szutu, D., Ribeiro, J.V., Verfaillie, J., Baldocchi, D., 2021. Evaluation of atmospheric boundary layer height from wind profiling radar and slab models and its responses to seasonality of land cover, subsidence, and advection. *J. Geophys. Res.* 126, e2020JD033775.
- Rigden, A.J., Salvucci, G.D., 2015. Evapotranspiration based on equilibrated relative humidity (ETRHEQ): Evaluation over the continental U.S. *Water Resour. Res.* 51 (4), 2951–2973.
- Rigden, A.J., Li, D., 2017. Attribution of surface temperature anomalies induced by land use and land cover changes. *Geophys. Res. Lett.* 44, 6814–6822.
- De Roo, F.D., Zhang, S., Huq, S., Mauder, M., 2018. A semi-empirical model of the energy balance closure in the surface layer. *PLoS One* 13 (12), e0209022.
- Salcido, A., Celada-Murillo, A.-T., Carreón-Sierra, S., Castro, T., Peralta, O., Salcido-González, R.-S., Hernández-Flores, N., Tamayo-Flores, G.-A., Martínez-Flores, M.-A., 2020. Estimations of the Mexicali Valley (Mexico) mixing height. *Atmosphere* 11 (5), 505.
- Salvucci, G.D., Gentile, P., 2013. Emergent relation between surface vapor conductance and relative humidity profiles yields evaporation rates from weather data. *Proc. Natl. Acad. Sci.* 110 (16), 6287–6291.
- Sanchez-Mejia, Z.M., Papuga, S.A., 2014. Observations of a two-layer soil moisture influence on surface energy dynamics and planetary boundary layer characteristics in a semiarid shrubland. *Water Resour. Res.* 50, 306–317.
- Sanchez-Mejia, Z.M., Papuga, S.A., 2017. Empirical modeling of planetary boundary layer dynamics under multiple precipitation scenarios using a two-layer soil moisture approach: an example from a semiarid shrubland. *Water Resour. Res.* 53, 8807–8824.
- Santanello, J.A., Dirmeyer, P.A., Ferguson, C.R., Findell, K.L., Tawfik, A.B., Berg, A., Ek, M., Gentile, P., Guillod, B.P., van Heerwaarden, C., Roundy, J., Wulfmeyer, V., 2018. Land-atmosphere interactions: the LoCo perspective. *Bull. Am. Meteorol. Soc.* 99 (6), 1253–1272.
- Santanello, J.A., Peters-Lidard, C.D., Kumar, S.V., 2011. Diagnosing the sensitivity of local land-atmosphere coupling via the soil moisture-boundary layer interaction. *J. Hydrometeorol.* 12 (5), 766–786.

- Santanello, J.A., Peters-Lidard, C.D., Kumar, S.V., Alonge, C., Tao, W., 2009. A modeling and observational framework for diagnosing local land-atmosphere coupling on diurnal time scales. *J. Hydrometeorol.* 10, 577–599.
- Schimel, D., Pavlick, R., Fisher, J.B., Asner, G.P., Saatchi, S., Townsend, P., Miller, C., Frankenberg, C., Hibbard, K., Cox, P., 2015. Observing terrestrial ecosystems and the carbon cycle from space. *Global Change Biol.* 21 (5), 1762–1776.
- Schmid, H.P., 1994. Source areas for scalars and scalar fluxes. *Boundary Layer Meteorol.* 67, 293–318.
- Schumacher, D.L., Keune, J., van Heerwaarden, C.C., 2019. Amplification of mega-heatwaves through heat torrents fuelled by upwind drought. *Nat. Geosci.* 12, 712–717.
- Seibert, P., Beyrich, F., Gryning, S.-E., Joffre, S., Rasmussen, A., Tercier, P., 2000. Review and intercomparison of operational methods for the determination of the mixing height. *Atmos. Environ.* 34 (7), 1001–1027.
- Seidel, D.J., Ao, C.O., Li, K., 2010. Estimating climatological planetary boundary layer heights from radiosonde observations: comparison of methods and uncertainty analysis. *J. Geophys. Res.* 115, D16113.
- Seneviratne, S.I., Corti, T., Davin, E.L., Hirschi, M., Jaeger, E.B., Lehner, I., Orlowsky, B., Teuling, A.J., 2010. Investigating soil moisture–climate interactions in a changing climate: a review. *Earth Sci. Rev.* 99 (3–4), 125–161.
- Serafin, S., Adler, B., Cuxart, J., De Wekker, S.F.J., Gohm, A., Grisogono, B., Kalthoff, N., Kirshbaum, D.J., Rotach, M.W., Schmidli, J., Stiperski, I., Véeneklaas, J., Zardi, D., 2018. Exchange processes in the atmospheric boundary layer over mountainous terrain. *Atmosphere* 9, 102.
- Shen, S., Leclerc, M.Y., 1995. How large must surface inhomogeneities be before they influence the convective boundary layer structure? A case study. *Q.J.R. Meteorol. Soc.* 121, 1209–1228.
- Shi, Y., Davis, K.J., Duffy, C.J., Yu, X., 2013. Development of a coupled land surface hydrologic model and evaluation at a critical zone observatory. *J. Hydrometeorol.* 14, 1401–1420.
- Shuttleworth, W.J., Serrat-Capdevila, A., Roderick, M.L., Scott, R.L., 2009. On the theory relating changes in area-average and pan evaporation. *Q. J. R. Meteorol. Soc.* 135 (642), 1230–1247.
- Sikma, M., Vilà-Guerau de Arellano, J., 2019. Substantial reductions in cloud cover and moisture transport by dynamic plant responses. *Geophys. Res. Lett.* 46 (3), 1870–1878.
- Sinclair, V.A., Belcher, S.E., Gray, S.L., 2010. Synoptic controls on boundary-layer characteristics. *Boundary Layer Meteorol.* 134, 387–409.
- Siqueira, M., Katul, G., Porporato, A., 2009. Soil moisture feedbacks on convection triggers: the role of soil-plant hydrodynamics. *J. Hydrometeorol.* 10 (1), 96–112.
- Steeneveld, G.-J., 2014. Current challenges in understanding and forecasting stable boundary layers over land and ice. *Front. Environ. Sci.* 2, 41.
- Stiperski, I., Holtslag, A.A.M., Lehner, M., Hoch, S.W., Whiteman, C.D., 2020. On the turbulence structure of deep katabatic flows on a gentle mesoscale slope. *Q. J. R. Meteorol. Soc.* 146, 1206–1231.
- Stoy, P.C., Mauder, M., Foken, T., Marcolla, B., Boegh, E., Ibrom, A., Arain, M.A., Arneth, A., Aurela, M., Bernhofer, C., Cescatti, A., Dellwik, E., Duce, P., Gianelle, D., van Gorsel, E., Kiely, G., Knohl, A., Margolis, H., McCaughey, H., Varlagin, A., 2013. A data-driven analysis of energy balance closure across FLUXNET research sites: The role of landscape scale heterogeneity. *Agric. For. Meteorol.* 171–172, 137–152.
- Stull, R.B., 1988. Mean boundary layer characteristics. In: Stull, R.B. (Ed.), *An Introduction to Boundary Layer Meteorology*. Springer, Netherlands, pp. 1–27.
- Styles, J.M., Lloyd, J., Zolotukhin, D., Lawton, K.A., Tchekakova, N., Francey, R.J., Arneth, A., Salamakha, D., Kolle, O., Schulze, E.-D., 2002. Estimates of regional surface carbon dioxide exchange and carbon and oxygen isotope discrimination during photosynthesis from concentration profiles in the atmospheric boundary layer. *Tellus B* 54, 768–783.
- Sugita, M., Hiyama, T., Kayane, I., 1997. How regional are the regional fluxes obtained from lower atmospheric boundary layer data? *Water Resour. Res.* 33 (6), 1437–1445.
- Sun, J., Lenschow, D.H., Mahrt, L., Crawford, T.L., Davis, K.J., Oncley, S.P., MacPherson, J.I., Wang, Q., Dobosy, R.J., Desjardins, R.L., 1997. Lake-induced atmospheric circulations during BOREAS. *J. Geophys. Res.* 102, 29155–29166.
- Sweeney, C., Karion, A., Wolter, S., Newberger, T., Guenther, D., Higgs, J.A., Andrews, A. E., Lang, P.M., Neff, D., Dlugokencky, E., Miller, J.B., Montzka, S.A., Miller, B.R., Masarie, K.A., Biraud, S.C., Novelli, P.C., Crotwell, M., Crotwell, A.M., Thoning, K., Tans, P.P., 2015. Seasonal climatology of CO<sub>2</sub> across North America from aircraft measurements in the NOAA/ESRL Global Greenhouse Gas Reference Network. *J. Geophys. Res.* 120 (10), 5155–5190.
- Tennekes, H., 1973. A model for the dynamics of the inversion above a convective boundary layer. *J. Atmosph. Sci.* 30, 558–567.
- Thomas, C., Foken, T., 2007. Flux contribution of coherent structures and its implications for the exchange of energy and matter in a tall spruce canopy. *Boundary Layer Meteorol.* 123 (2), 317–337.
- Tucker, S.C., Senff, C.J., Weickmann, A.M., Brewer, W.A., Banta, R.M., Sandberg, S.P., Law, D.C., Hardesty, R.M., 2009. Doppler lidar estimation of mixing height using turbulence, shear, and aerosol profiles. *J. Atmos. Oceanic Technol.* 26 (4), 673–688.
- van Heerwaarden, C.C., Teuling, A.J., 2013. Disentangling the response of forest and grassland energy exchange to heatwaves under idealized land-atmosphere coupling. *Biogeosciences* 11, 6159–6171.
- van Heerwaarden, C.C., Vilà-Guerau de Arellano, J., Moene, A.F., Holtslag, A.A.M., 2009. Interactions between dry-air entrainment, surface evaporation and convective boundary-layer development. *Q. J. R. Meteorol. Soc.* 135 (642), 1277–1291.
- van Stratum, B.J.H., Vilà-Guerau de Arellano, J., van Heerwaarden, C.C., Ouwersloot, H. G., 2014. Subcloud-layer feedbacks driven by the mass flux of shallow cumulus convection over land. *J. Atmospheric Sci.* 71 (3), 881–895.
- Venkatram, A., 1977. A model of internal boundary-layer development. *Boundary Layer Meteorol.* 11 (4), 419–437.
- Vesala, T., Kljun, N., Rannik, Ü., Rinne, J., Sogachev, A., Markkanen, T., Sabelfeld, K., Foken, Th., Leclerc, M.Y., 2008. Flux and concentration footprint modelling: State of the art. *Environ. Pollut.* 152 (3), 653–666.
- Vick, E.S.K., Stoy, P.C., Tang, A.C.I., Gerken, T., 2016. The surface-atmosphere exchange of carbon dioxide, water, and sensible heat across a dryland wheat-fallow rotation. *Agricul. Ecosyst. Environ.* 232, 129–140.
- Vickers, D., Mahrt, L., 2004. Evaluating formulations of stable boundary layer height. *J. Appl. Meteorol.* 43, 1736–1749.
- Vilà-Guerau de Arellano, J., Ney, P., Hartogensis, O., de Boer, H., van Diepen, K., Emin, D., de Groot, G., Klosterhalfen, A., Langensiepen, M., Matveeva, M., Miranda-García, G., Moene, A.F., Rascher, U., Röckmann, T., Adnew, G., Brügmann, N., Rothfuss, Y., Graf, A., 2020. CloudRoots: integration of advanced instrumental techniques and process modelling of sub-hourly and sub-kilometre land-atmosphere interactions. *Biogeosciences* 17, 4375–4404.
- Vila-Guerau de Arellano, J., van Heerwaarden, C., van Stratum, B.J.H., van den Dries, K., 2015. *Atmospheric Boundary Layer: Integrating Air Chemistry and Land Interactions*. Cambridge University Press.
- Vilà-Guerau de Arellano, J., Ouwersloot, H.G., Baldocchi, D., Jacobs, C.M.J., 2014. Shallow cumulus rooted in photosynthesis. *Geophys. Res. Lett.* 41 (5), 1796–1802.
- Vilà-Guerau de Arellano, J., van Heerwaarden, C.C., Lelieveld, J., 2012. Modelled suppression of boundary-layer clouds by plants in a CO<sub>2</sub>-rich atmosphere. *Nat. Geosci.* 5 (10), 701–704.
- Vilà-Guerau de Arellano, J., Gioli, B., Miglietta, F., Jonker, H.J.J., Baltink, H.K., Huitjes, R.W.A., Holtlag, A.A.M., 2004. Entrainment process of carbon dioxide in the atmospheric boundary layer. *J. Geophys. Res.* 109, D18110.
- Vogel, M.M., Orth, R., Cheruy, F., Hagemann, S., Lorenz, R., Hurk, B.J.J.M., Seneviratne, S.I., 2017. Regional amplification of projected changes in extreme temperatures strongly controlled by soil moisture–temperature feedbacks. *Geophys. Res. Lett.* 44 (3), 1511–1519.
- Wang, W., Davis, K.J., Cook, B.D., Yi, C., Butler, M.P., Ricciuto, D.M., Bakwin, P.S., 2007. Estimating daytime CO<sub>2</sub> fluxes over a mixed forest from tall tower mixing ratio measurements. *J. Geophys. Res.* 112, D10308.
- Wang, W., Davis, K.J., Ricciuto, D.M., Butler, M.P., 2006. An approximate footprint model for flux measurements in the convective boundary layer. *J. Atmos. Oceanic Technol.* 23 (10), 1384–1394.
- Wang, X.Y., Wang, K.C., 2014. Estimation of atmospheric mixing layer height from radiosonde data. *Atmos. Meas. Tech.* 7 (6), 1701–1709.
- Wesely, M.L., 1976. The combined effect of temperature and humidity fluctuations on refractive index. *J. Appl. Meteorol.* 15 (1), 43–49.
- Wesloh, D., Lauvaux, T., Davis, K.J., 2020. Development of a mesoscale inversion system for estimating continental-scale CO<sub>2</sub> fluxes. *J. Adv. Model. Earth Syst.* 12, e2019MS001818.
- Wharton, S., Ma, S., Baldocchi, D.D., Falk, M., Newman, J.F., Osuna, J.L., Bible, K., 2017. Influence of regional nighttime atmospheric regimes on canopy turbulence and gradients at a closed and open forest in mountain-valley terrain. *Agric. For. Meteorol.* 237–238, 18–29.
- White, A.B., Fairall, C.W., Thomson, D.W., 1991. Radar observations of humidity variability in and above the marine atmospheric boundary layer. *J. Atmos. Oceanic Technol.* 8 (5), 639–658.
- Wilczak, J.M., Gossard, E.E., Neff, W.D., Eberhard, W.L., 1996. Ground-based remote sensing of the atmospheric boundary layer: 25 years of progress. *Boundary Layer Meteorol.* 78 (3), 321–349.
- Wilson, J.D., Swaters, G.E., 1991. The source area influencing a measurement in the planetary boundary layer: the “footprint” and the “distribution of contact distance”. *Boundary Layer Meteorol.* 55, 25–46.
- Wofsy, S.C., Harriss, R.C., Kaplan, W.A., 1988. Carbon dioxide in the atmosphere over the Amazon Basin. *J. Geophys. Res.* 93 (D2), 1377–1387.
- Wolf, S., Keenan, T.F., Fisher, J.B., Baldocchi, D.D., Desai, A.R., Richardson, A.D., Scott, R.L., Law, B.E., Litvak, M.E., Brunsell, N.A., Peters, W., van der Laan-Luijkx, I. T., 2016. Warm spring reduced carbon cycle impact of the 2012 US summer drought. *Proc. Natl. Acad. Sci.* 113 (21), 5880–5885.
- Wood, C.R., Järvi, L., Kouznetsov, R.D., Nordbo, A., Joffre, S., Drebs, A., Vihma, T., Hirsimäki, A., Suomi, I., Fortelius, C., O'Connor, E., Moiseev, D., Haapanala, S., Moilanen, J., Kangas, M., Karppinen, A., Vesala, T., Kukkonen, J., 2013. An overview of the urban boundary layer atmosphere network in Helsinki. *Bull. Am. Meteorol. Soc.* 94 (11), 1675–1690.
- Wouters, H., Petrova, I.Y., van Heerwaarden, C.C., Vilà-Guerau de Arellano, J., Teuling, A.J., Meulenbergh, V., Santanello, J.A., Miralles, D.G., 2019. Atmospheric boundary layer dynamics from balloon soundings worldwide: CLASS4GL v1.0. *Geosci. Model Devol.* 12, 2139–2153.
- Wulfmeyer, V., Hardesty, R.M., Turner, D.D., Behrendt, A., Cadeddu, M.P., Di Girolamo, P., Schlüssel, P., Van Baelen, J., Zus, F., 2015. A review of the remote sensing of lower-tropospheric thermodynamic profiles and its indispensable role for the understanding and the simulation of water and energy cycles. *Rev. Geophys.* 53, 819–895.
- Wulfmeyer, V., Späth, F., Behrendt, A., Jach, L., Warrach-Sagi, K., Ek, M., Turner, D.D., Senff, C., Ferguson, C.R., Santanello, J., Lee, T.R., Buban, M., Verhoef, A., 2020. The GEWEX Land-Atmosphere Feedback Observatory (GLAFO). *GEWEX Q.* 30 (1), 6–11.
- Wulfmeyer, V., Turner, D.D., Baker, B., Banta, R., Behrendt, A., Bonin, T., Brewer, W.A., Buban, M., Choukulkar, A., Dumas, E., Hardesty, R.M., Heus, T., Ingwersen, J., Lange, D., Lee, T.R., Metzendorf, S., Muppa, S.K., Meyers, T., Newsom, R., Osman, M., Raasch, S., Santanello, J., Senff, C., Späth, F., Wagner, T., Weckwerth, T., 2018. New research approach for observing and characterizing land-atmosphere feedback. *Bull. Am. Meteorol. Soc.* 99, 1639–1667.

- Wyngaard, J.C., Brost, R.A., 1984. Top-down and bottom-up diffusion of a scalar in the convective boundary layer. *J. Atmospheric Sci.* 41 (1), 102–112.
- Xiao, J.F., Davis, K.J., Urban, N.M., Keller, K., 2014a. Uncertainty in model parameters and regional carbon fluxes: A model-data fusion approach. *Agric. For. Meteorol.* 189–190, 175–186.
- Xiao, J., Ollinger, S.V., Frolking, S., Hurtt, G.C., Hollinger, D.Y., Davis, K.J., Pan, Y., Zhang, X., Deng, F., Chen, J., Baldocchi, D.D., Law, B.E., Arain, M.A., Desai, A.R., Richardson, A.D., Sun, G., Amiro, B., Margolis, H., Gu, L., Scott, R.L., Blanken, P.D., Suyker, A.E., 2014b. Data-driven diagnostics of terrestrial carbon dynamics over North America. *Agric. For. Meteorol.* 197, 142–157.
- Xu, K., Metzger, S., Desai, A.R., 2017. Upscaling tower-observed turbulent exchange at fine spatio-temporal resolution using environmental response functions. *Agric. For. Meteorol.* 232, 10–22.
- Xu, K., Sühring, M., Metzger, S., Durden, D., Desai, A.R., 2020. Can data mining help eddy covariance see the landscape? A large-eddy simulation study. *Boundary Layer Meteorol.* <https://doi.org/10.1007/s10546-020-00513-0>.
- Yi, C., Davis, K.J., Bakwin, P.S., Berger, B.W., Marr, L.C., 2000. Influence of advection on measurements of the net ecosystem-atmosphere exchange of CO<sub>2</sub> from a very tall tower. *J. Geophys. Res.* 105 (D8), 9991–9999. <https://doi.org/10.1029/2000JD900080>.
- Yi, C., Davis, K.J., Bakwin, P.S., Denning, A.S., Zhang, N., Desai, A., Lin, J.C., Gerbig, C., 2004. Observed covariance between ecosystem carbon exchange and atmospheric boundary layer dynamics at a site in northern Wisconsin. *J. Geophys. Res.* 109 (D8), 9991–9999.
- Yi, C., Davis, K.J., Berger, B.W., Bakwin, P.S., 2001. Long-term observations of the dynamics of the continental planetary boundary layer. *J. Atmospheric Sci.* 58, 1288–1299.
- Yin, J., Gao, C.Y., Hong, J., Gao, Z., Li, Y., Li, X., Fan, S., Zhu, B., 2019. Surface meteorological conditions and boundary layer height variations during an air Pollution episode in Nanjing, China. *J. Geophys. Res.* 124 (6), 3350–3364.
- Yin, J., Albertson, J.D., Rigby, J.R., Porporato, A., 2015. Land and atmospheric controls on initiation and intensity of moist convection: CAPE dynamics and LCL crossings. *Water Resour. Res.* 51 (10), 8476–8493.
- Zhao, M., Heinsch, F.A., Nemani, R.R., Running, S.W., 2005. Improvements of the MODIS terrestrial gross and net primary production global data set. *Remote Sens. Environ.* 95 (2), 164–176.
- Zhou, Y., Williams, C.A., Lauvaux, T., Davis, K.J., Feng, S., Baker, I., Denning, S., Wei, Y., 2020. A multiyear gridded data ensemble of surface biogenic carbon fluxes for North America: evaluation and analysis of results. *J. Geophys. Res.* 125, e2019JG005314.
- Zilitinkevich, S.S., Tyurakov, S.A., Troitskaya, Yu.I., Mareev, E.A., 2012. Theoretical models of the height of the atmospheric boundary layer and turbulent entrainment at its upper boundary. *Izvestiya, Atmosph. Oceanic Phys.* 48 (1), 133–142.
- Zilitinkevich, S., Baklanov, A., 2002. Calculation of the height of the stable boundary layer in practical applications. *Boundary Layer Meteorol.* 105, 389–409.